Chromomycin Dimer–DNA Oligomer Complexes. Sequence Selectivity and Divalent Cation Specificity†

Xiaolian Gao and Dinshaw J. Patel*

Department of Biochemistry and Molecular Biophysics, College of Physicians and Surgeons, Columbia University, New York, New York 10032

Received June 4, 1990; Revised Manuscript Received August 27, 1990

ABSTRACT: This paper reports on a solution NMR characterization of the sequence selectivity and metal ion specificity in chromomycin–DNA oligomer complexes in the presence of divalent cations. The sequence selectivity studies have focused on chromomycin complexes with the self-complementary d(A1-A2-G3-G4-C5-C6-T7-T8) duplex containing a pair of adjacent (G3-G4)·(C5-C6) steps and the self-complementary d(A1-G2-G3-A4-T5-C6-C7-T8) duplex containing a pair of separated (G2-G3)·(C6-C7) steps in aqueous solution. The antitumor agent (chromomycin) and nucleic acid protons have been assigned following analysis of distance connectivities in NOESY spectra and coupling connectivities in DQF-COSY spectra for both complexes in H_2O and D_2O solution. The observed intermolecular NOEs establish that chromomycin binds as a Mg(II)-coordinated dimer [1 Mg(II) per complex] and contacts the minor-groove edge with retention of 2-fold symmetry centered about the (G3-G4-C5-C6)·(G3-G4-C5-C6) segment of the $d(A_2G_2C_2T_2)$ duplex. By contrast, complex formation is centered about the (G2-G3-A4-T5)·(A4-T5-C6-C7) segment and results in removal of the two fold symmetry of the $d(AG_2ATC_2T)$ duplex. Thus, the binding of one subunit of the chromomycin dimer at its preferred (G-G)·(C-C) site assists in the binding of the second subunit to the less preferred adjacent (A-T)·(A-T) site. These observations suggest a hierarchy of chromomycin binding sites, with a strong site detected at the (G-G) step due to the hydrogen-bonding potential of acceptor N3 and donor NH_2 groups of guanosine that line the minor groove. The divalent cation specificity has been investigated by studies on the symmetric chromomycin–$d(A_2G_2C_2T_2)$ complex in the presence of diamagnetic Mg(II), Zn(II), and Cd(II) cations and paramagnetic Ni(II) and Co(II) cations. A comparative NOESY study of the Mg(II) and Ni(II) symmetric complexes suggests that a single tightly bound divalent cation aligns the two chromomycins in the dimer through coordination to the C1 carbonyl and C9 enolate ions on the hydrophilic edge of each aglycon ring. Secondary divalent cation binding sites involve coordination to the major-groove N7 atoms on adjacent guanosines in G-G steps. This coordination is perturbed on lowering the pH below 6.0, presumably due to protonation of the N7 atoms. The midpoint of the thermal dissociation of the symmetric complex is dependent on the divalent cation with the stability for reversible transitions decreasing in the order Mg(II) > Zn(II) > Cd(II) complexes. We have also measured the real-time proton to deuterium exchange kinetics of the aglycon C8-hydroxyl proton in the symmetric chromomycin–d-$(A_2G_2C_2T_2)$ complex after dissolution in D_2O solution. The hydrogen exchange lifetimes in the absence of added catalysts decreases in the order Ni(II) ≫ Mg(II) > Zn(II) > Cd(II) complexes. The same trend is detected for divalent cation exchange between the tightly bound and free cations, with the bound Ni(II) exhibiting the longest and the bound Cd(II) the shortest lifetime in the symmetric complex. These results establish that the divalent cation exchange does not occur through direct penetration of the cation into the complex but rather following dissociation of the divalent cation coordinated chromomycin dimer from its duplex binding site.

Chromomycin **1** belongs to the aureolic group of antibiotics (Gause, 1974), which are highly effective antitumor agents against a wide variety of experimental and human tumors (Kennedy et al., 1968). Chromomycin **1**, which contains an aglycon chromophore and five attached hexapyranoses (Miyamoto et al., 1964; Thiem & Meyer, 1979; Chart I), selectively inhibits DNA-dependent RNA synthesis through formation of DNA complexes in the presence of Mg(II) ions (Ward et al., 1965). Early research suggested binding at guanosine residues in DNA, and this specificity is retained in antibiotics lacking one or more sugar residues (Behr et al., 1969).

Chemical (Van Dyke & Dervan, 1983) and nuclease (Fox & Howarth, 1985) digestion studies have elucidated the sequence specificity associated with the binding of chromomycin to DNA. Methidiumpropyl-EDTA–Fe(II) footprinting studies have established that chromomycin and a related antibiotic, mithramycin, exhibit similar sequence specificities with a minimum site size of three base pairs containing at least two contiguous G·C base pairs (Van Dyke and Dervan, 1983). Related footprinting studies with DNase I established chromomycin and mithramycin binding sites at sequences containing two contiguous G·C base pairs with (G-G)·(C-C) as the preferred dinucleotide step (Fox & Haworth, 1985; Cons & Fox, 1989). Further, the bound antitumor agent enhances DNase I cleavage rates at flanking sequences containing runs of A and T residues.

Two NMR studies have been reported on chromomycin–DNA oligomer complexes with diametrically opposite conclusions. It was initially claimed that chromomycin bound as

† This research was supported by NIH CA-46778. X.G. was supported in part by a Special Fellowship of the Leukemia Society of America. The NMR spectrometers were purchased from funds donated by the Robert Woods Johnson Jr. Trust and the Matheson Trust toward setting up an NMR Center in the Basic Medical Sciences at Columbia University.

0006-2960/90/0429-10940$02.50/0

Chart I

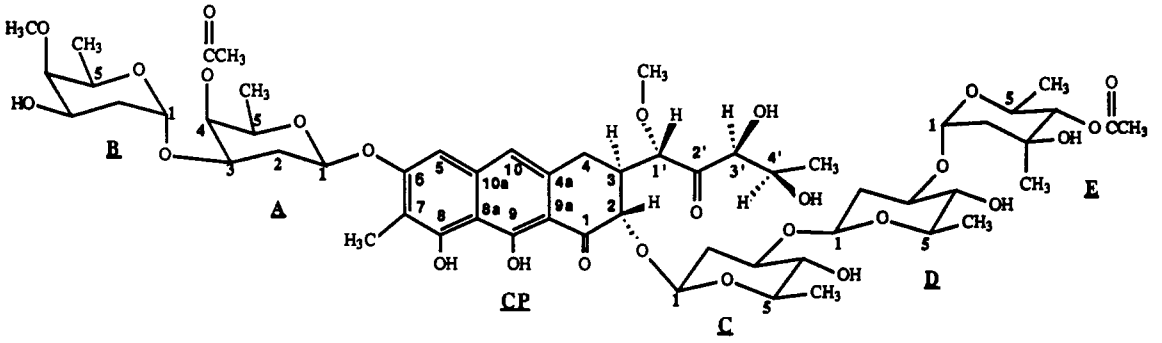

Chromomycin -A_3

1

a *monomer* in the *major* groove to *one strand* of the self-complementary d(A-T-G-C-A-T) duplex (Keniry et al., 1987). By contrast, our studies established that chromomycin bound as a divalent metal ion coordinated *dimer* to G·C-rich segments in the *minor* groove and switched the conformation to a wider and shallower minor groove at its (G-G-C-C-A)·(G-G-C-C-A) binding site on *both strands* of the self-complementary d(T-T-G-G-C-C-A-A) duplex (Gao & Patel, 1989). The analysis and interpretations by Keniry et al. (1987) reflected their addition of only 1 equiv of chromomycin per duplex, and hence they were unknowingly investigating a mixture of free duplex and a complex containing 2 chromomycins per duplex. This group has now reinterpreted their experimental NMR data (Banville et al., 1990) and have adopted our published model for the chromomycin–DNA complex in solution (Gao & Patel, 1989).

We have continued our research on chromomycin–DNA oligomer complexes, with this paper addressing questions related to the sequence selectivity and divalent cation specificity in chromomycin–DNA complex formation. The sequence selectivity studies focus on a comparative investigation of chromomycin binding to the self-complementary d(A1-A2-G3-G4-C5-C6-T7-T8) duplex and to the self-complementary d(A1-G2-G3-A4-T5-C6-C7-T8) duplex [1 Mg(II) and 2 drug molecules per duplex] in aqueous solution. The former duplex contains the preferred (G3-G4)·(C5-C6) half-sites adjacent to each other, while the latter duplex contains the preferred (G2-G3)·(C6-C7) half-sites separated by two A·T pairs. The divalent cation specificity studies focus on the formation and stability of the chromomycin–d($A_2G_2C_2T_2$) complex in the presence of diamagnetic Mg(II), Zn(II), and Cd(II) cations as well as paramagnetic Ni(II) and Co(II) cations.

Experimental Procedures

Oligonucleotide Synthesis. The self-complementary d(A-A-G-G-C-C-T-T) and d(A-G-G-A-T-C-C-T) octanucleotides were synthesized on a 10-μmol scale on a Beckman System 1 Plus synthesizer. The general procedures for deprotection and purification by reverse-phase HPLC have been reported previously (Gao & Jones, 1987).

Sequence Selectivity Studies. The samples of the chromomycin–DNA oligomer complexes for two-dimensional NMR studies were in the 3–4 mM concentration range and were generated by addition of 2 equiv of chromomycin to 1 equiv of the self-complementary octanucleotide duplex in the presence of 1 equiv of Mg(II) cation. The buffer was 0.1 M NaCl and 10 mM phosphate in aqueous solution.

Metal Ion Specificity Studies. The initial sample contained 0.4–0.8 mM in double strand of d($A_2G_2C_2T_2$) and >2 equiv of chromomycin in 0.4 mL of 0.1 M NaCl and 10 mM phosphate buffer solution. The complexes were generated by addition of chloride salts of different divalent metal ions from stock solutions at μmol/μL concentration. Complex formation was monitored in the proton spectrum by following the disappearance of resonances from the free octamer duplex and the appearance of resonances from the complex.

NMR Experiments. One- and two-dimensional proton NMR spectra were recorded on Bruker AM-400 and AM-500 spectrometers. Two-dimensional NMR data sets were processed by using FTNMR software (Hare Research).

One-dimensional NOE difference experiments were collected in H_2O by using the 1-1 H_2O suppression pulse. The carrier frequency was shifted 4000 Hz downfield from the H_2O resonance and the 1-1 delay optimized for solvent suppression. We collected 2048 complex data points over a 30 ppm sweep width with a 1.2-s repetition delay. Resonances of interest were irradiated for 400 ms with the decoupler channel. Data sets corresponding to on- and off-resonance irradiation were interleaved every 32 scans for a total of 1600–3200 scans. The free induction decays were subtracted after applying a line broadening of 3 Hz and Fourier transformed to obtain the NOE difference spectra.

Two-dimensional phase-sensitive NOESY spectra (mixing time 110 ms) in H_2O were recorded by using a jump and return pulse sequence for the detection pulse. The carrier frequency was centered on the H_2O signal and the waiting time, t, was 70–90 μs. The time domain data sets consist of 1024 complex data points over a sweep width of 25 ppm in the t_2 dimension. The repetition delay was 1.0 s. The free induction decays were apodized with a skewed sine bell function in both the t_2 and t_1 dimensions before Fourier transformation. Each dimension was baseline corrected, with data points of the water signal set to zero.

Correlated spectra (DQF-COSY) were recorded in the phase-sensitive mode in D_2O solution. Time domain data sets, consisting of 256–300 t_1 increments, were collected with a sweep width of 8–10 ppm by using 1024 complex data points in the t_2 dimension and a repetition delay of 1.5–2 s. A total of 32–64 scans were collected for each t_1 increment. These data were apodized with a sine bell function in both the t_2 and t_1 dimensions prior to Fourier transformation.

Two-dimensional homonuclear Hartmann–Hahn (HOHAHA) spectra were recorded in D_2O solution with a 35-ms spin lock time. The time domain data sets were accumulated over a sweep width of 10 ppm by using 1024 and 256 complex data points in t_2 and t_1 dimensions, respectively. We collected 64–96 scans for each increment with a repetition delay of 2

s. The free induction decays were apodized with a skewed sine bell function in both the t_2 and t_1 dimensions prior to Fourier transformation.

Two-dimensional phase-sensitive NOESY spectra were recorded in D_2O solution. The time domain data sets were accumulated over a sweep width of 10 ppm by using 1024 complex data points in the t_2 dimension and 256 increments in the t_1 dimension. The repetition delay was 2.0 s, and 32–64 scans were collected for each t_1 increment. The free induction decays were apodized with a sine bell function in both the t_2 and t_1 dimensions before Fourier transformation. Each dimension was baseline corrected with a polynomial baseline fitting routine.

Two-dimensional heteronuclear phosphorus-detected ^{31}P–^1H phase-sensitive relay COSY spectra were recorded by using a modified HETCOR pulse sequence and processed as reported (Zagorski & Norman, 1988).

The proton spin–lattice relaxation times ($T1$) were measured from nonselective inversion recovery experiments on the complex in D_2O with a repetition delay at least 4 times the longest $T1$ in the complex.

The aglycon C8-hydroxyl and G3 imino proton resonances are well resolved in all the complexes reported in this paper, and their intensities were used to monitor the dissociation and exchange process of the complex. Use of the intensity as a marker for monitoring the dissociation of the complex is justified by the observation of constant line widths of these exchangeable protons throughout the melting process.

Thermal Melting Studies. The temperature-dependent spectra were recorded automatically every 15 min with temperature increments of 2–3 °C. The melting profiles for individual chromomycin–d($A_2G_2C_2T_2$) complexes as a function of divalent cation were recorded by monitoring the intensity of the resolved aglycon C8-hydroxyl proton and the guanosine imino protons in the complex.

Metal Ion Exchange Kinetics. Real-time exchange of the aglycon C8-hydroxyl in the complex as a function of divalent cation could be measured by dissolving a fully protonated sample into D_2O buffer and monitoring either absolute or relative peak intensities as a function of time.

The observed exchange between two different divalent cations can be described by the equation

$$Z + M(CHR) \underset{k_M}{\overset{k_Z}{\rightleftharpoons}} Z(CHR) + M \qquad (1)$$

In this equation, Z and M are the free metal cations, Z(CHR) and M(CHR) are the corresponding chromomycin–DNA complexes, and k_Z and k_M are rate constants for free Z cation replacing M in M(CHR) and free M cation replacing Z in Z(CHR), respectively. The formation rate of M(CHR) can be expressed as

$$d[M(CHR)]/dt = k_M[M][Z(CHR)] - k_Z[Z][M(CHR)] \qquad (2)$$

In the presence of excess M, the formation of M(CHR) follows first-order kinetics [initial M(CHR) concentration is negligible]. Thus, the exchange time constant can be derived from the exponential buildup of the intensity of the M(CHR) resonance as a function of time.

Results

Symmetric Mg(II)-Coordinated Chromomycin–d($A_2G_2C_2T_2$) Complex

Stoichiometry and Symmetry of Complex. The proton NMR spectrum of the chromomycin–d($A_2G_2C_2T_2$) complex [1 Mg(II) and 2 drug molecules per duplex] in H_2O buffer, pH 4.6, at 15 °C is plotted in Figure 1A. The exchangeable protons in the spectrum include the nucleic acid imino (12.0–14.5 ppm) and amino (6.0–10.0 ppm) protons and the chromomycin hydroxyl proton (16.2 ppm). The observation of four imino protons establishes that the self-complementary d($A_2G_2C_2T_2$) duplex retains its 2-fold element of symmetry on complex formation with 2 equiv of added chromomycin.

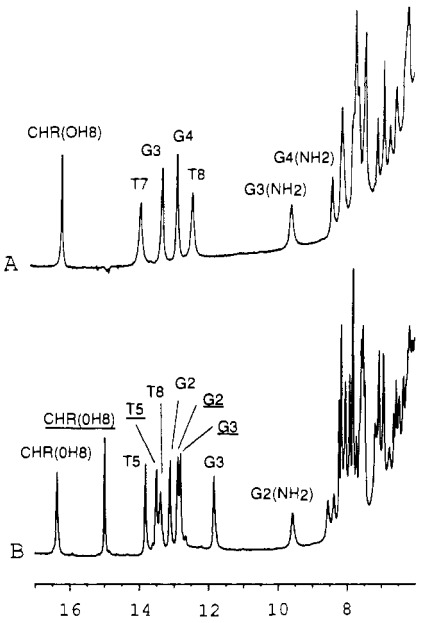

FIGURE 1: Exchangeable proton spectra (6–17 ppm) of (A) the chromomycin–d($A_2G_2C_2T_2$) complex [1 Mg(II) and 2 drug molecules per duplex], pH 4.6, 15 °C and (B) the chromomycin–d(AG_2ATC_2T) complex [1 Mg(II) and 2 drug molecules per duplex], pH 7.4, 7 °C. The buffer contained 0.1 M NaCl, 10 mM phosphate, and 0.1 mM EDTA in H_2O solution.

The proton-decoupled phosphorus spectrum of the chromomycin–d($A_2G_2C_2T_2$) complex [1 Mg(II) and 2 drug molecules per duplex] in D_2O buffer, pH 6.0, at 25 °C is plotted in Figure S1A (see supplementary material). The observation of seven partially resolved phosphorus resonances reinforces the conclusion that the 2-fold symmetry of the self-complementary d($A_2G_2C_2T_2$) duplex is retained on complex formation with 2 equiv of chromomycin.

We have only detected resonances of the free duplex and that of the complex containing 2 chromomycins per duplex on gradual addition of chromomycin to d($A_2G_2C_2T_2$) duplex in buffer solution containing 1 equiv of Mg(II) ion. There was no evidence for formation of intermediate states containing 1 chromomycin bound to the d($A_2G_2C_2T_2$) duplex.

Imino and Amino Proton Assignments. The exchangeable protons in the d($A_2G_2C_2T_2$) duplex and its chromomycin complex have been assigned by a combination of one- and two-dimensional NOE experiments under conditions of solvent suppression. The one-dimensional NOE data on the complex were collected at pH 6.3, 2 °C, and at pH 4.6, 15 °C, and are plotted in Figures S2 and S3, respectively (supplementary material). We focus below on the NOESY spectrum (110-ms mixing time) of the chromomycin–d($A_2G_2C_2T_2$) complex [1 Mg(II) and 2 drug molecules per duplex] in H_2O buffer, pH 4.6, at 15 °C. The expanded region establishing distance connectivities between imino protons and chromomycin hydroxyl protons (12.0–16.5 ppm) and the amino, base, and sugar H1′ protons (5.2–9.8 ppm) is plotted in Figure 2A, and the symmetrical expanded region about 5.2–9.8 ppm is plotted in Figure 2B. The relevant labeled NOE cross peak assignments are listed in the caption to Figure 2, and the chemical shifts are summarized in Table I. The most interesting feature of

Table I: Proton Chemical Shifts (ppm) in the Chromomycin–d($A_2G_2C_2T_2$) Complex [1 Mg(II) and 2 Drug Molecules per Duplex][a]

d($A_2G_2C_2T_2$) Protons													
nucleotide	NH	NH_2		H8	H2	H6	H5	H1′	H2′	H2″	H3′	H4′	H5′,5″
A1				7.77	7.69			5.89	2.47	2.62	4.82	4.15	3.68
A2				8.06	7.68			5.93	2.77	2.74	4.98	4.40	4.14
G3	13.18	9.48	6.30	7.45				6.17	2.97	2.32	4.65	4.26	
G4	12.67	8.17	6.34[b]	6.98				5.62	2.75	2.32	4.11	3.77	3.97
C5		8.13	6.82			7.06	5.16	5.59	2.10	1.67	4.09	1.59	3.24 3.54
C6		8.23	6.67			7.64	5.45	6.26	2.53	2.37	4.64	4.63	3.49 4.14
T7	14.07					7.71	1.64	6.33	2.28	2.54	4.91	4.16	3.90 4.05
T8	12.89					7.44	1.64	6.23	2.20	2.22	4.53	3.92	4.04

Chromomycin Saccharide Protons									
sugar	H1	H2(a)	H2(e)	H3	H4	H5	H6	Ac	OCH_3
A	5.68	2.09	2.35	4.34	5.28	4.10	1.36	2.34	
B	5.15	1.77	1.50	4.05	3.47	3.85	1.24		3.53
C	4.84	1.79	2.44	2.30	2.91	2.84	1.19		
D	2.67	1.12	2.21	3.68	2.96	3.16	1.19		
E	5.16	2.47	2.09	1.51	5.21	4.30	1.66	2.24	

Chromomycin Aglycon Protons												
aglycon	H2	H3	H4(a,e)	H5	H7	H10	H1′	H1′(OMe)	H3′	H4′	H5′	OH8
CHR	4.60	2.72	2.77 2.51	6.87	2.68	6.56	4.91	3.35	4.17	4.22	1.26	16.15

[a] Buffer solution contains 0.1 M NaCl, 10 mM phosphate, and 6 mM $MgCl_2$. The nonexchangeable proton data were obtained in D_2O, pH 6.7, at 25 °C; the exchangeable proton data were obtained in H_2O, pH 6.3, at 2 °C. [b] Assigned from D_2O spectrum.

this expanded NOESY contour plot is the observation of four exchangeable proton cross peaks between each guanosine imino proton and the amino protons within the G·C pairs (Figure 2A).

The 12.81 ppm imino proton of G4 exhibits cross peaks to protons located at 8.38 (cross peak I, Figure 2A), 8.04 (cross peak H, Figure 2A), 6.87 (cross peak G, Figure 2A), and 6.50 ppm (cross peak F, Figure 2A) in the expanded NOESY spectrum of the complex. A cross peak is detected between the 8.38 and 6.50 ppm resonances (cross peak B, Figure 2B), defining these as one pair of amino protons, while a cross peak is detected between the 8.04 and 6.87 ppm resonances (cross peak D, Figure 2B), defining these as a second set of amino protons. In addition, the 8.38 ppm hydrogen-bonded and 6.50 ppm exposed amino protons each exhibit NOEs to the 6.25 ppm sugar H1′ protons of C6 (cross peaks F and H, Figure 2B) and to the 5.55 ppm sugar H1′ proton of C5 (cross peaks E and G, Figure 2B). The guanosine amino protons at position 2 of G·C base pairs are located in the minor groove, and NOEs are predicted to sugar H1′ protons, also located in the minor groove. This permits assignment of the 8.38 and 6.50 ppm resonances to the hydrogen-bonded and exposed minor-groove amino protons of G4, while the 8.04 and 6.87 ppm resonances must then be assigned to the hydrogen-bonded and exposed major-groove amino protons of C5 within the G4·C5 base pair in the complex.

The 13.24 ppm imino proton of G3 exhibits cross peaks to protons located at 9.53 (cross peak E, Figure 2A), 8.11 (cross peak D, Figure 2A), 6.70 (cross peak C, Figure 2A), and 6.28 ppm (cross peak B, Figure 2A) in the expanded NOESY spectrum of the complex. The 9.53 and 6.28 ppm resonances are linked by an NOE (cross peak A, Figure 2B), defining these as one pair of amino protons, while the 8.11 and 6.70 ppm resonances are linked by an NOE (cross peak C, Figure 2B), defining these as a second set of amino protons. These latter amino protons at 8.11 and 6.70 ppm each exhibit NOEs to the 5.48 ppm H5 proton of C6 (cross peaks I and J, Figure 2B). This permits assignment of the 8.11 and 6.70 ppm exchangeable resonances to the hydrogen-bonded and exposed major-groove amino protons of C6, while the 9.53 and 6.28 ppm exchangeable protons must then be assigned to the hydrogen-bonded and exposed amino protons of G3 within the G3·C6 base pair.

Thus, the amino protons of G4 and C5 within the G4·C5 base pair and the amino protons of G3 and C6 within the G3·C6 base pair exhibit resolved hydrogen-bonded and exposed resonances for the complex in pH 4.6 buffer solution at 15 °C (Figures 1A and 2). These shifts exhibit a small dependence on pH and provide markers in the minor (guanosine amino protons) and major (cytidine amino protons) grooves for monitoring chromomycin–nucleic acid interactions.

The chemical shifts of the exchangeable protons in the d($A_2G_2C_2T_2$) duplex are listed in Table SI (supplementary material), and those in the Mg(II)-coordinated chromomycin–d($A_2G_2C_2T_2$) complex are listed in Table I.

Intermolecular NOEs Involving Exchangeable Protons. The observation of a single aglycon hydroxyl proton at 16.15 ppm in the Mg(II)-coordinated chromomycin–d($A_2G_2C_2T_2$) complex suggests that the second chromomycin hydroxyl proton is ionized in solution. The observed NOE between the 2.63 ppm chromomycin C7-CH_3 proton and the 16.15 ppm resonance permits assignment of the downfield exchangeable resonance to the C8-hydroxyl proton in the complex. The 16.15 ppm aglycon C8-hydroxyl proton exhibits weak NOEs to the 8.38 ppm hydrogen-bonded and 6.50 ppm exposed amino protons of G4 (cross peaks J and K, Figure 2A), to the superpositioned exposed amino proton of G3 and the H1′ proton of C6 (cross peak L, Figure 2A), and to the H1′ proton of C5 (cross peak M, Figure 2A).

We detect intermolecular NOE cross peaks between C7-CH_3 protons and the imino and hydrogen-bonded amino protons of G3. A weaker NOE was also observed between the C7-CH_3 protons and the hydrogen-bonded amino proton of G4.

Nonexchange Proton Spectra. The one-dimensional proton NMR spectrum (1.0–8.5 ppm) of the chromomycin–d($A_2G_2C_2T_2$) complex [1 Mg(II) and 2 drug molecules per duplex] in D_2O buffer, pH 6.7, at 25 °C is plotted in Figure S4A (supplementary material). The nonexchangeable protons are well resolved in this spectrum and have been assigned following analysis of through-space distance connectivities in the 250-ms NOESY (cross peaks to the right of the diagonal in Figure S4B) and through-bond coupling connectivities in DQF-COSY (cross peaks to the left of the diagonal in Figure S4B) two-dimensional data sets.

The experimental one- and two-dimensional proton spectra

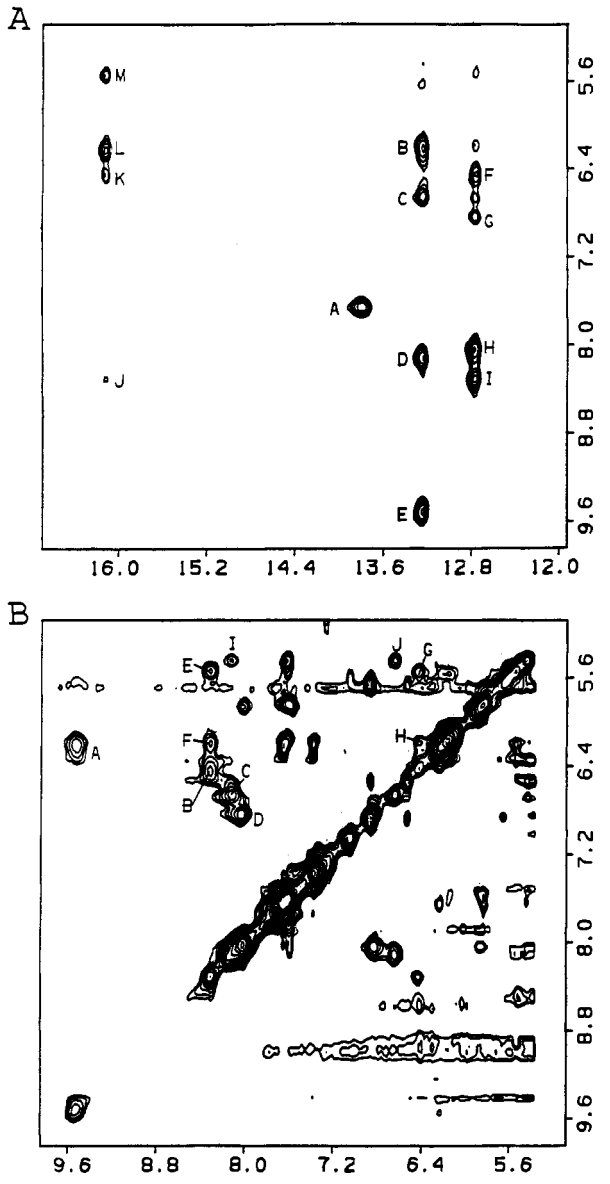

FIGURE 2: (A) An expanded contour plot establishing distance connectivities between the 12.0–16.5 ppm and 5.4–9.6 ppm regions in the phase-sensitive NOESY spectrum (110-ms mixing time) of the Mg(II)-coordinated chromomycin–d($A_2G_2C_2T_2$) complex in H_2O buffer, pH 4.6, at 15 °C. The cross peaks A–M are assigned as follows: A, T7(NH)–A2(H2); B, G3(NH)–G3(NH_2e); C, G3(NH)–C6(NH_2e); D, G3(NH)–C6(NH_2b); E, G3(NH)–G3(NH_2b); F, G4(NH)–G4(NH_2e); G, G4(NH)–C5(NH_2e); H, G4(NH)–C5(NH_2b); I, G4(NH)–G4(NH_2b); J, CHR(OH8)–G4(NH_2b); K, CHR(OH8)–G4(NH_2e); L, CHR(OH8)–C6(H1′); and M, CHR(OH8)–C5(H1′). (B) An expanded contour plot establishing distance connectivities within the symmetrical 5.4–9.6 ppm region in the phase-sensitive NOESY spectrum (110-ms mixing time) of the Mg(II)-coordinated chromomycin–d($A_2G_2C_2T_2$) complex in H_2O buffer, pH 4.6, at 15 °C. The cross peaks A–J are assigned as follows: A, G3(NH_2b)–G3(NH_2e); B, G4(NH_2b)–G4(NH_2e); C, C6(NH_2b)–C6(NH_2e); D, C5(NH_2b)–C5(NH_2e); E, G4(NH_2b)–C5(H1′); F, G4(NH_2b)–C6(H1′); G, G4(NH_2e)–C5(H1′); H, G4(NH_2e)–C6(H1′); I, C6(NH_2b)–C6(H5); and J, C6(NH_2e)–C6(H5).

establish that the 2-fold symmetry of the d($A_2G_2C_2T_2$) duplex is retained on complex formation with 2 equiv of chromomycin in aqueous solution.

Nucleic Acid Nonexchangeable Proton Shifts. An expanded 250-ms NOESY contour plot establishing distance connectivities between the base protons (6.9–8.3 ppm) and the sugar H1′ and cytidine H5 protons (5.0–6.4 ppm) in the chromomycin–d($A_2G_2C_2T_2$) complex, 25 °C, is shown in Figure 3A. We detect NOEs between the base protons and

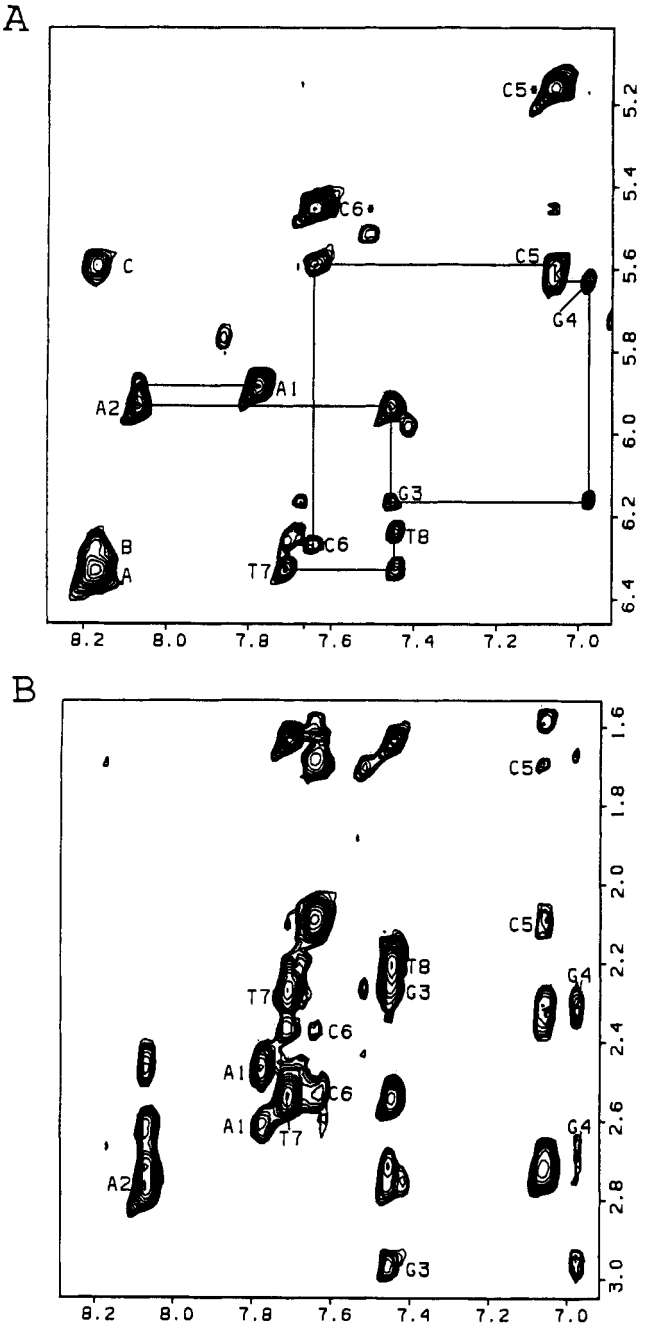

FIGURE 3: Expanded NOESY (250-ms mixing time) contour plots establishing distance connectivities for the Mg(II)-coordinated chromomycin–d($A_2G_2C_2T_2$) complex in D_2O buffer, pH 6.7, at 25 °C. (A) Cross peaks connecting the base and slowly exchanging amino protons (6.9–8.3 ppm) with the sugar H1′ and cytidine H5 protons (5.1–6.4 ppm). (B) Cross peaks connecting the base and slowly exchanging amino protons (6.9–8.3 ppm) with the sugar H2′,2″ protons (1.5–3.1 ppm). The cross peaks A–C are assigned as follows: A, G4(NH_2b)–G4(NH_2e); B, G4(NH_2b)–C6(H1′); and C, G4(NH_2b)–C5(H1′).

their own and 5′-flanking sugar H1′ protons so that the chain can be traced from A1 to T8 as outlined in Figure 3A. We detect a cross peak (labeled A in Figure 3A) between the 8.17 ppm hydrogen-bonded and 6.34 ppm exposed amino protons of G4 and between the hydrogen-bonded amino proton of G4 and the H1′ protons of C5 (peak C, Figure 3A) and C6 (peak B, Figure 3A).

An expanded 250-ms NOESY contour plot establishing distance connectivities between the base protons (6.9–8.3 ppm) and the sugar H2′,2″ and thymidine CH_3 protons (1.5–3.1 ppm) in the chromomycin–d($A_2G_2C_2T_2$) complex, 25 °C, is

Table II: Proton Chemical Shift Differences (ppm) upon Chromomycin–d($A_2G_2C_2T_2$) Complex Formation

	d($A_2G_2C_2T_2$) Protons[a]										
nucleotide	NH	NH_2		H8	H2	H6	H5	H1′	H2′	H2″	H3′	H4′
A1				0.07	−0.06			−0.15	−0.24	−0.21	−0.11	−0.08
A2				−0.01	−0.01			−0.18	−0.10	−0.03	−0.05	−0.10
G3	−0.32			0.12				−0.64	−0.47	0.25	0.24	0.04
G4	0.25			0.62				0.22	−0.26	0.30	0.76	0.58
C5		−0.07	−0.44			0.23	−0.01	0.29	0.00	0.75	0.63	2.57
C6		0.10	0.29			−0.15	0.04	−0.38	−0.44	−0.28	0.06	−0.54
T7	0.01					−0.21	0.02	−0.19	−0.02	−0.05	−0.09	0.00
T8	0.01					0.04	0.02	−0.03	0.03	0.01	−0.02	0.08

	Chromomycin Saccharide Protons[b]								
sugar	H1	H2(a)	H2(e)	H3	H4	H5	H6	Ac	OCH_3
A	−0.37	0.04	−0.27	−0.30	−0.11	−0.28	−0.10		
B	−0.12	0.23	0.52	−0.15	−0.27	0.01	0.00		
C	0.33	0.05	0.15	1.42	0.19	0.51	0.14		
D	2.14	0.67	0.26	−0.06	0.18	0.19	0.16		
E	0.05	−0.76	−0.08	−0.13	−0.46	−0.26	−0.41		

	Chromomycin Aglycon Protons											
aglycon	H2	H3	H4(a,e)	H5	H7	H10	H1′	H1′(OMe)	H3′	H4′	H5′	OH8
CHR	0.19	−0.09	0.37 0.18	−0.29	−0.37	0.17	−0.20		0.16	0.18	0.07	−0.40

[a] Difference = δ(free) − δ(complex) under similar experimental conditions. A minus value indicates a downfield shift upon complex formation. [b] Difference = δ(free in CD_2Cl_2) − δ(complex). A minus value indicates a downfield shift upon complex formation in aqueous solution. Free chromomycin chemical shifts in CD_2Cl_2 at 23 °C are from Thiem and Meyer (1979). These chemical shift differences are not corrected for solvent contributions.

shown in Figure 3B. The base (purine H8 and pyrimidine H6) protons exhibit NOEs to their own and 5′-flanking sugar H2′,2″ protons, with the former cross peaks labeled in Figure 3B. We note that the base protons of G4, C5, and C6 exhibit stronger NOEs to their 5′-flanking sugar H2′,2″ protons relative to their own sugar H2′,2″ protons in the complex (Figure 3B). This is most readily visualized by comparing one-dimensional slices taken through the base protons of G4, C5, and C6 (Figure S5, panels A, B, and C, respectively, in the supplementary material) with the slice taken through the base proton of A2 (Figure S4, panel D).

The expanded NOESY plots in Figure 3 yield the proton chemical shifts of the base, H1′, and H2′,2″ protons in the complex, and a similar investigation of other expanded regions such as that between the H1′ and H3′ protons (4.0–6.4 ppm) and the H2′,2″ and thymidine CH_3 protons (1.5–3.1 ppm), shown in Figure 4A, yields the H3′, H4′, and a few of the H5′,5″ proton assignments in the complex. The nonexchangeable nucleic acid base and sugar proton chemical shifts in the Mg(II)-coordinated chromomycin–d($A_2G_2C_2T_2$) complex at 25 °C are listed in Table I.

Parallel two-dimensional NOESY and DQF-COSY data sets have also been recorded on the d($A_2G_2C_2T_2$) duplex in D_2O buffer, pH 6.4, at 25 °C. The data sets are of sufficient quality to yield the base and sugar proton assignments for the free duplex listed in Table SI (supplementary material).

The nonexchangeable proton complexation shifts on proceeding from the free d($A_2G_2C_2T_2$) duplex (Table SI) to the Mg(II)-coordinated chromomycin–d($A_2G_2C_2T_2$) complex (Table I) are listed in Table II. The largest nonexchangeable proton complexation shift is detected at H4′ of C5 (2.57 ppm), followed by H8 of G4 (0.62 ppm), H2″ of C5 (0.75 ppm), H3′ of G4 (0.76 ppm), H3′ of C5 (0.63 ppm), and H4′ of G4 (0.58 ppm). The largest downfield complexation shifts are detected at H2′ of G3 (−0.47 ppm), H2′ of C6 (−0.44 ppm), and H4′ of C6 (−0.54 ppm) (Table II).

Nucleic Acid Proton Coupling Constants. An expanded contour plot of the DQF-COSY spectrum establishing coupling connectivities between the sugar H1′ and H3′ protons (4.0–6.4 ppm) and the sugar H2′,2″ protons (1.5–3.2 ppm) in the chromomycin–d($A_2G_2C_2T_2$) complex in D_2O buffer at 35 °C is plotted in Figure 4B. We note distinct differences in cross

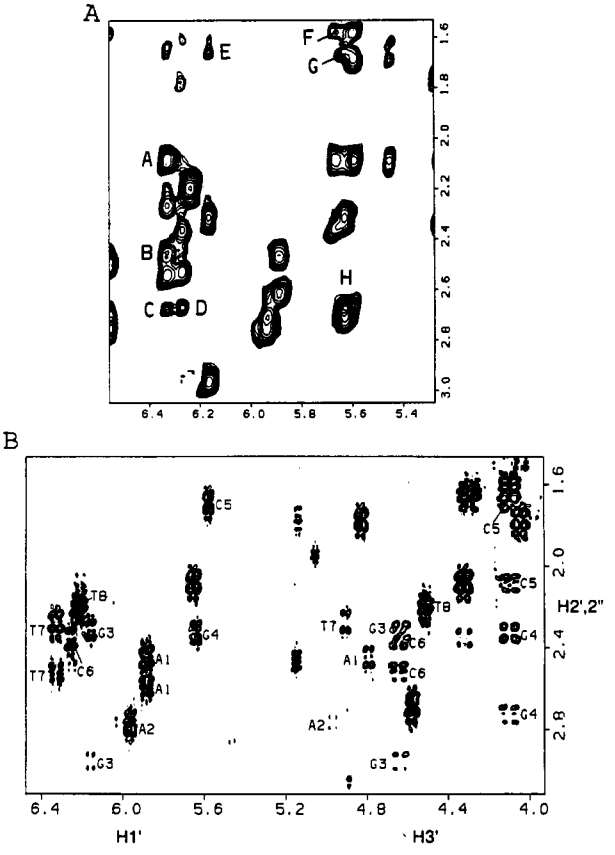

FIGURE 4: Expanded contour plots of (A) the 250-ms NOESY spectrum, pH 6.7, at 25 °C and (B) the DQF-COSY spectrum at 35 °C for the Mg(II)-coordinated chromomycin–d($A_2G_2C_2T_2$) complex in D_2O buffer. The cross peaks A–H are assigned as follows: A, E(H2e)–T7(H1′); B, E(H2a)–T7(H1′); C, CHR(C7-CH_3)–G4-(NH_2e); D, CHR(C7-CH_3)–C6(H1′); E, E(C6-CH_3)–G3(H1′); F, A(H1)–C5(H4′); G, E(C6-CH_3)–G4(H1′); and H, CHR(C7-CH_3)–G4(H1′).

peak patterns for the central G3-G4-C5-C6 segment relative to the flanking A1-A2 and T7-T8 segments in the complex. Thus, the H1′ protons of A1 and T7 exhibit equally strong cross peaks to their H2′ and H2″ protons, and a similar pattern is assumed for A2 and T8, where the H2′ and H2″ protons

Table III: Proton–Proton Vicinal Coupling Constants of Chromomycin–d($A_2G_2C_2T_2$) Complex

nucleotide	coupling constants (Hz)[a]				
	1′2′	1′2″	3′2′	3′2″	3′4′
A1	8	6	+	–	w
A2	8	6	+	–	w
G3	5	6	+	+	s
G4	2	8	+	+	s
C5	1	8	+	+	s
C6	3	8	+	+	*b*
T7	9	7	+	–	w
T8	*b*	*b*	*b*	*b*	m

[a] w, m, and s represent weak, moderate, and strong coupled spins. + and – signs represent those coupling cross peaks that were observed and not observed, respectively. [b] Proton pairs are overlapped.

are superpositioned (Figure 4B). By contrast, the H1′ proton of G3 exhibits a stronger coupling cross peak to the H2″ proton relative to the H2′ proton of G3, while the H1′ protons of G4, C5, and C6 exhibit coupling connectivities to their H2″ protons but not their H2′ protons (Figure 4B). The same distinction between the central segment and the flanking segment is detected for the coupling connectivities between the H3′ protons and the H2′,2″ protons in the complex. Thus, for A1 and T7 (and presumably A2 and T8), the H3′ proton exhibits a coupling connectivity to the H2′ but not the H2″ proton (Figure 4B). By contrast, the H3′ protons of G3, G4, C5, and C6 exhibit coupling connectivities to both the H2′ and H2″ protons. The estimated vicinal proton–proton sugar coupling constants in the chromomycin dimer–d($A_2G_2C_2T_2$) complex at 35 °C are listed in Table III.

A parallel DQF-COSY study has been undertaken on the d($A_2G_2C_2T_2$) duplex with an expanded contour plot establishing coupling connectivities between the sugar H1′ and H3′ protons and the H2′,2″ protons plotted in Figure S6 (supplementary material). All the sugars in the duplex exhibit similar patterns, with vicinal couplings detected for H1′–H2′, H1′–H2″, and H3′–H2′ but not H3′–H2″ connectivities (Figure S6). The estimated vicinal proton–proton sugar coupling constants in the d($A_2G_2C_2T_2$) duplex at 25 °C are listed in Table SII (supplementary material).

Chromomycin Nonexchangeable Proton Shifts. Chromomycin **1** contains an aglycon ring to which are attached a hydrophilic side chain at position 3, a disaccharide (rings A and B) at position 6, and a trisaccharide (rings C, D, and E) at position 2. The antitumor drug protons have been assigned following analysis of NOESY, DQF-COSY, and HOHAHA two-dimensional data sets on the chromomycin–d($A_2G_2C_2T_2$) complex in D_2O buffer at 25 °C. An expanded 250-ms NOESY contour plot establishing distance connectivities in the symmetrical 1.0–5.8 ppm region is plotted in Figure S7 (supplementary material). We outline the tracing of NOE connectivities within the C-sugar ring (cross peaks to the left of the diagonal in Figure S7) and the D-sugar ring (cross peaks to the right of the diagonal in Figure S7) in the C-D-E trisaccharide segment. The same procedures can be used to assign the protons in the A-B disaccharide segment, the aglycon, and the hydrophilic side chain of chromomycin in the complex. The magnitudes (weak, medium, and strong intensity) of the observed intraresidue NOEs for the chromomycin components (A-, B-, C-, D- and E-sugars, aglycon, and hydrophilic side chain) in the complex are tabulated in Table SIII (supplementary material), and the magnitudes of the interresidue NOEs between chromomycin components in the complex are tabulated in Table SIV (supplementary material).

The nonexchangeable chromomycin proton chemical shifts in the Mg(II)-coordinated chromomycin–d($A_2G_2C_2T_2$) complex at 25 °C are listed in Table I, and the complexation shifts on proceeding from chromomycin in methylene chloride to the complex in D_2O solution are listed in Table II. The largest upfield nonexchangeable proton complexation shifts are detected at the H2 equatorial proton of the B-sugar (0.52 ppm), the H3 proton of the C-sugar (1.42 ppm), the H5 proton of the C-sugar (0.51 ppm), the H1 proton of the D-sugar (2.14 ppm), and the H2 axial proton of the D-sugar (0.67 ppm). The largest downfield nonexchangeable proton complexation shifts are detected at H4 (–0.46 ppm) and H6 (–0.41 ppm) of the E-sugar (Table II).

Table IV: Intermolecular NOEs in the Chromomycin–d($A_2G_2C_2T_2$) Complex

chromomycin residue		d($A_2G_2C_2T_2$)						
		residue	H2	H1′	H2′	H2″	H4′	H5′,5″
A-sugar[a]	H1	G4					w	
	H1	C5					w	
	H1	C5						w
	H2a	G4					w	
	H2e	G4					m	
aglycon[b]	H5	G4				w		
	H5	C5					w	w
	CH_3-7	G4		s				
	CH_3-7	C5		w	w			
	OH8	C5		w				
	OH8	C6		w				
	H10	C5					m	w
C-sugar[c]	H2a	C6		w				
	H2e	C6		w			w	
	H4	C6					w	
D-sugar[d]	H2a	T7					m	w
	H2e	T7		w			w	
E-sugar[e]	H1	T7		m			w	
	H2a	T7		s			w	
	H2a	A2	w					
	H2e	T7		s			w	
	CH_3-3	T7		w				
	H4	G3		w				
	H4	T7		w				
	CH_3-6	G3		w				
	CH_3-6	G4		m			w	
	OAc	G3					w	

[a] Chromomycin A-sugars interact with the backbone of d($A_2G_2C_2T_2$) at the G4-C5 step. [b] Each of the aglycons binds to the G3·C6 and the G4·C5 pairs with its hydrophilic edge facing the minor groove and its hydrophobic edge tilted toward the backbone. [c] Chromomycin C-sugars are located at the cross section of the chromomycin dimer and show weak contacts with the C6 residue in the minor groove of d($A_2G_2C_2T_2$). [d] Chromomycin D-sugars are stacked over the aglycon rings and show weak contacts with the T7 residue in the minor groove of d($A_2G_2C_2T_2$). [e] Chromomycin E-sugars, which reside in the minor groove at the G3·C6 and A2·T7 pairs, exhibit NOEs to protons of the T7 and cross-strand G3 and G4 residues. E-sugars are oriented with their geminal H2 protons pointing toward the H1′ protons of the T7 residues and with their C6 methyls directed toward the G3 residues on the opposite strands.

Intermolecular NOEs Involving Nonexchangeable Protons. The intermolecular NOEs between chromomycin protons and the d($A_2G_2C_2T_2$) duplex protons in the complex can be readily identified once the NOEs within individual components have been assigned and the proton chemical shifts documented as listed in Table I. An expanded 250-ms mixing time NOESY spectrum of the chromomycin–d($A_2G_2C_2T_2$) complex at 25 °C establishing distance connectivities between the 5.2–6.6 ppm and 1.4–3.2 ppm regions is plotted in Figure 4A. Several intermolecular NOEs can be identified in this expanded plot; the assignments are listed in the caption to Figure 4A. The intermolecular NOEs are defined as weak, medium, and strong and are summarized in Table IV.

The strongest nonexchangeable proton intermolecular NOEs are detected between the C7-CH_3 protons of the aglycon and

FIGURE 5: Nonexchangeable proton spectra (6.5–8.5 ppm) of the Mg(II)-coordinated chromomycin–d($A_2G_2C_2T_2$) complex. (A) Spectrum at pH 6.0. (B) Spectrum at pH 4.8. Chemical shift assignments were made by two-dimensional data analysis. (C) Excess Mg(II) added; spectrum at pH 5.0. (D) Excess paramagnetic Mn(II) added; spectrum at pH 4.8.

the H1′ proton of G4 (peak H, Figure 4A) and between the H2a/H2e protons of the E-sugar and the H1′ proton of T7 (peaks A and B, Figure 4A) in the complex. Medium-intensity nonexchangeable proton intermolecular NOEs are detected between the H2e proton of the A-ring and the H4′ proton of G4, between the H1 proton of the E-ring and the H1′ proton of T7, and between the CH_3-6 proton of the E-ring and the H1′ proton of G4 (peak G, Figure 4A).

Phosphorus Spectra. Seven partially resolved phosphorus resonances are detected in phosphorus spectra of the d-($A_2G_2C_2T_2$) duplex and the chromomycin–d($A_2G_2C_2T_2$) complex (Figure S1A) in D_2O buffer at 25 °C with the spectral dispersion of 0.5 ppm in the duplex increasing to 1.7 ppm in the complex (Figure S1A). Three phosphorus resonances shift to high field and two phosphorus resonances shift to low field on complex formation.

The phosphorus resonances in the chromomycin–d-($A_2G_2C_2T_2$) complex have been assigned following analysis of a two-dimensional heteronuclear phosphorus-detected phosphorus–proton phase-sensitive relay COSY data set. The corresponding contour plot establishing through bond and relay coupling connectivities between the phosphorus resonances and the sugar H3′, H2′,2″, and H4′ protons in the O3′ direction and the sugar H5′,5″ and H4′ protons in the O5′ direction is plotted in Figure S8A (supplementary material). The connectivities can be readily monitored by recording one-dimensional slices through individual phosphorus resonances as shown in Figure S8B (supplementary material) for the 3.66 ppm G3–G4 phosphorus resonance in the complex. The phosphorus resonances can be assigned on the basis of the known sugar proton assignments in the Mg(II)-coordinated chromomycin–d($A_2G_2C_2T_2$) complex; these assignments are made in Figure S1A and listed in Table SV.

pH Dependence of Proton Spectra in Complex. Proton spectra of the chromomycin–d($A_2G_2C_2T_2$) complex [1 Mg(II) and 2 drug molecules per duplex] in D_2O buffer have been recorded at pH 4.8 and 6.0 at 25 °C. The largest chemical shift changes are observed at the nucleic acid H8 protons of G3 and G4 in the complex, which shift to low field on decreasing the pH from 6.0 (Figure 5A) to 4.8 (Figure 5B).

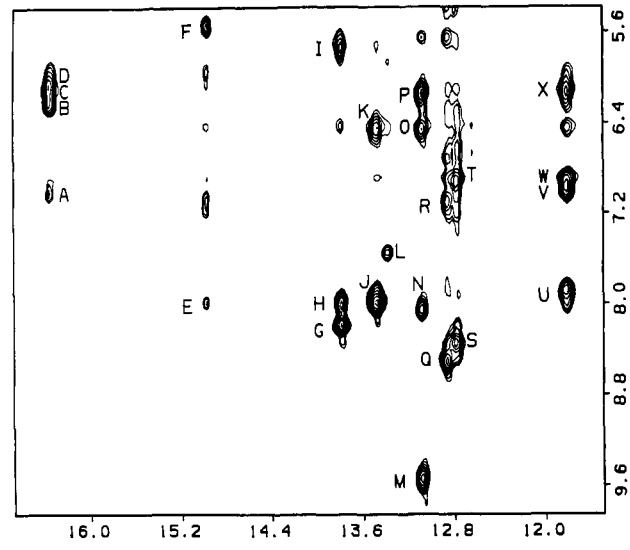

FIGURE 6: An expanded NOESY contour plot (110-ms mixing time) establishing distance connectivities between the 11.5–16.0 ppm and 5.5–9.6 ppm regions for the Mg(II)-coordinated chromomycin–d-(AG_2ATC_2T) complex in H_2O buffer, pH 7.4, at 5 °C. The cross peaks A–X are assigned as follows: A, CHR(OH8)–G3(NH_2b); B, CHR(OH8)–G2(H1′); C, CHR(OH8)–G3(NH_2e); D, CHR-(OH8)–A4(H1′); E, CHR(OH8)–A4(H2); F, CHR(OH8)–C6(H1′); G, T5(NH)–A4(H2); H, T5(NH)–A4(H2); I, T5(NH)–A4(NH_2e); J, T5(NH)–A4(H2); K, T5(NH)–A4(NH_2e); L, T8(NH)–A1(H2); M, G2(NH)–G2(NH_2b); N, G2(NH)–C7(NH_2b); O, G2(NH)–C7(NH_2e); P, G2(NH)–G2(NH_2e); Q, G2(NH)–C7(NH_2b); R, G2(NH)–C7(NH_2e); S, G3(NH)–C6(NH_2b); T, G3(NH)–C6-(NH_2e); U, G3(NH)–C6(NH_2b); V, G3(NH)–G3(NH_2b); W, G3-(NH)–C6(NH_2e); and X, G3(NH)–G3(NH_2e).

These pH-dependent shifts are characteristic of the complex since they were not detected in the free d($A_2G_2C_2T_2$) duplex.

Asymmetric Mg(II)-Coordinated Chromomycin–d(AG_2ATC_2T) Complex

Asymmetry of Complex. The proton spectrum of the chromomycin–d(AG_2ATC_2T) complex [1 Mg(II) and 2 drug molecules per duplex] in H_2O solution, pH 7.4, at 7 °C is plotted in Figure 1B. We detect resolved C8-hydroxyl aglycon protons at 15.0 and 16.4 ppm and seven of the eight imino protons of the octanucleotide duplex between 11.5 and 14.0 ppm. These data establish that the binding of 2 equiv of chromomycin lifts the 2-fold symmetry of the exchangeable proton spectrum of the self-complementary d(AG_2ATC_2T) duplex. The two deoxyoctanucleotide strands in the complex are therefore nonequivalent and are differentiated by normal and underlined lettering in the text below.

The proton-decoupled phosphorus spectrum of the chromomycin–d(AG_2ATC_2T) complex [1 Mg(II) and 2 drug molecules per duplex] in D_2O buffer, pH 7.4, at 25 °C is plotted in Figure 2B. The observation of 14 partially resolved phosphorus resonances reinforces the conclusion that the 2-fold symmetry of the d(AG_2ATC_2T) duplex is lifted on complex formation with 2 equiv of chromomycin.

Imino and Amino Proton Assignments. The exchangeable protons resonating between 9 and 17 ppm in the proton spectrum of the Mg(II)-coordinated chromomycin–d-(AG_2ATC_2T) complex (Figure 1B) have been assigned from one-dimensional NOE and two-dimensional NOESY experiments in H_2O buffer. An expanded contour plot of the 110-ms NOESY spectrum of the complex establishing distance connectivities between the 11.5–16.5 ppm and 5.2–9.6 ppm regions at 5 °C is shown in Figure 6. The labeled cross peaks have been assigned and are listed in the caption to Figure 6.

Table V: Proton Chemical Shifts (ppm) in the Chromomycin–d(AG_2ATC_2T) Complex [1 Mg(II) and 2 Drug Molecules per Duplex][a]

d(AG_2ATC_2T) Protons													
nucleotide	NH	NH_2		H8	H2	H6	H5	H1′	H2′	H2″	H3′	H4′	H5′,5″
A1				8.14	7.64			5.95	2.66	2.78	4.70	4.06	3.79
A1				7.88	7.84			5.83	2.25	2.42	4.73	3.99	
G2	13.06	9.54	6.14	7.56				6.18	2.29	3.02	4.22		
G2	12.84			7.78				5.35	2.67		4.92	4.28	
G3	11.80	7.01	6.12	7.00				5.68	2.30	2.92		3.79	
G3	12.77			7.76				5.77	2.66	2.77	5.01	4.38	
A4		6.44		7.45	7.99			6.08	2.33		4.23	1.67	3.31 3.66
A4		5.74		8.09	8.18			6.33	2.53	3.00	5.02		
T5	13.78					7.59	0.86	6.46	2.10	2.62	4.80		
T5	13.46					7.00	1.49	6.05	2.06	2.71	4.77	4.00	
C6		8.33	6.91			7.47	5.48	6.12	2.01	2.46	4.89	3.75	
C6		7.86	6.88			7.14	5.43	5.55	2.06	2.47	4.08	1.54	
C7		8.46	7.07			7.54	5.67	6.05	2.26	2.40	4.83	4.10	
C7		8.04	6.44			7.45	5.23	6.24	2.15	2.45	4.58	4.54	
T8	13.37					7.50	1.71	6.19	2.25		4.50	4.04	
T8						7.68	1.51	6.31	2.12	2.19	4.53	3.95	

Chromomycin Saccharide Protons									
sugar	H1	H2(a)	H2(e)	H3	H4	H5	H6	Ac	OCH_3
A	5.57	2.09	2.34	4.37	5.31	4.11	1.38	2.34	
A	5.46	2.06	2.58	4.18	5.21	4.09	1.35	2.22	
B	5.16	1.47	1.77	4.03	3.57	3.97	1.33		3.57
B	5.10	1.55	1.77	4.04	3.48	3.85	1.25		3.53
C						2.83	1.22		
C						2.67	1.21		
D	2.65	0.99	2.47	3.52	2.87	3.28	1.23		
D	2.50	1.12	2.11	3.86	3.01	3.54	1.25		
E	5.24	2.15		1.52	5.15	4.29	1.65	2.26	
E	5.15	2.11	2.43	1.46	4.82	4.17	1.46	2.16	

Chromomycin Aglycon Protons												
aglycon	H3	H4(a,e)		H5	H7	H10	H1′	H1′(OMe)	H3′	H4′	H5′	OH8
CHR	2.65	2.44	2.48	6.88	2.62	6.60	5.00	3.35	4.13	4.22	1.22	14.95
CHR	2.85	2.62	2.75	6.88	2.46	6.52	4.82	3.35	4.15	4.24	1.26	16.34

[a] Buffer solution contained 0.1 M NaCl, 10 mM phosphate, and 12 mM $MgCl_2$. The nonexchangeable proton data were obtained in D_2O, pH 7.4, at 25 °C; the exchangeable proton data were obtained in H_2O, pH 7.4, at 5 °C. The assignments for H2′ vs H2″, H2(a) vs H2(e), H3 vs H4(a,e), and strand I vs strand II (underlined) are arbitrary in some cases.

The 13.06 ppm imino proton of G2 exhibits NOEs to its own hydrogen-bonded and exposed amino protons (peaks M and P, Figure 6) and to those of C7 (peaks N and O, Figure 6). Similarly, the 11.80 ppm imino proton of G3 exhibits NOEs to its own hydrogen-bonded and exposed amino protons of G3 (peaks V and X, Figure 6) and to those of C6 (peaks U and W, Figure 6). By contrast, the 12.84 ppm imino proton of G2 and the 12.77 ppm imino proton of G3 exhibit NOEs only to the hydrogen-bonded and exposed amino protons of C7 (peaks Q and R, Figure 6) and C6 (peaks S and T, Figure 6), respectively. These cross peak patterns establish slow rotation about the C–NH_2 bond of guanosines G2 and G3 but not G2 and G3 in the chromomycin–d(AG_2ATC_2T) complex.

The chemical shifts of the exchangeable protons in the d(AG_2ATC_2T) duplex are listed in Table SVI (supplementary material), and those in the Mg(II)-coordinated chromomycin–d(AG_2ATC_2T) complex are listed in Table V.

Intermolecular Contacts Involving Exchangeable Protons. Further characterization of the asymmetric binding of two chromomycin molecules to the d(A-G-G-A-T-C-C-T)·d(A-G-G-A-T-C-C-T) duplex is manifested in the observed intermolecular NOEs between the C8-hydroxyl protons on the aglycon of chromomycin and minor-groove proton markers on the DNA octanucleotide. The 16.34 ppm C8-hydroxyl proton exhibits NOEs to the hydrogen-bonded and exposed amino protons of G3 (peaks A and C, Figure 6) and to the H1′ protons of G2 (peak B, Figure 6) and A4 (peak D, Figure 6). The 14.95 ppm C8-hydroxyl proton exhibits NOEs to the H2 proton of A4 (peak E, Figure 6) and the H1′ proton of C6 (peak F, Figure 6).

Nonexchangeable Proton Spectra. The proton spectrum (1.0–8.5 ppm) of the chromomycin–d(AG_2ATC_2T) complex [1 Mg(II) and 2 drug molecules per duplex] in D_2O buffer, pH 7.4, at 25 °C is plotted in Figure S9A (supplementary material). The proton resonances are reasonably well resolved, though we observe twice as many resonances in the complex containing 2 equiv of chromomycin per self-complementary d(AG_2ATC_2T) duplex (Figure S9A) compared with the self-complementary d($A_2G_2C_2T_2$) duplex (Figure S4A).

The two-dimensional NOESY spectrum of the chromomycin–d(AG_2ATC_2T) complex (Figure S9B) exhibits twice the number of cross peaks as their counterparts in the chromomycin–d($A_2G_2C_2T_2$) complex (Figure S4B). These results establish that the 2-fold symmetry of the self-complementary d(AG_2ATC_2T) duplex is lifted on complex formation with the 2 equiv of chromomycin in aqueous solution. Therefore, the two strands of the octanucleotide duplex in the complex are distinguished by labeling them with normal and underlined print.

Nucleic Acid Nonexchangeable Proton Shifts. The nucleic acid base and sugar protons in the chromomcyin–d(AG_2ATC_2T) complex have been assigned following analysis of cross peaks in NOESY and DQF-COSY contour plots (Figure S9B). An example of this analysis is shown in the expanded 250-ms NOESY contour plots establishing distance connectivities between the base protons (7.2–8.2 ppm) and the sugar H1′ and cytidine H5 protons (5.2–6.6 ppm) in the complex plotted in duplicate in Figure 7. The chain tracing is drawn for the d(A1-G2-G3-A4-T5-C6-C7-T8) strand in

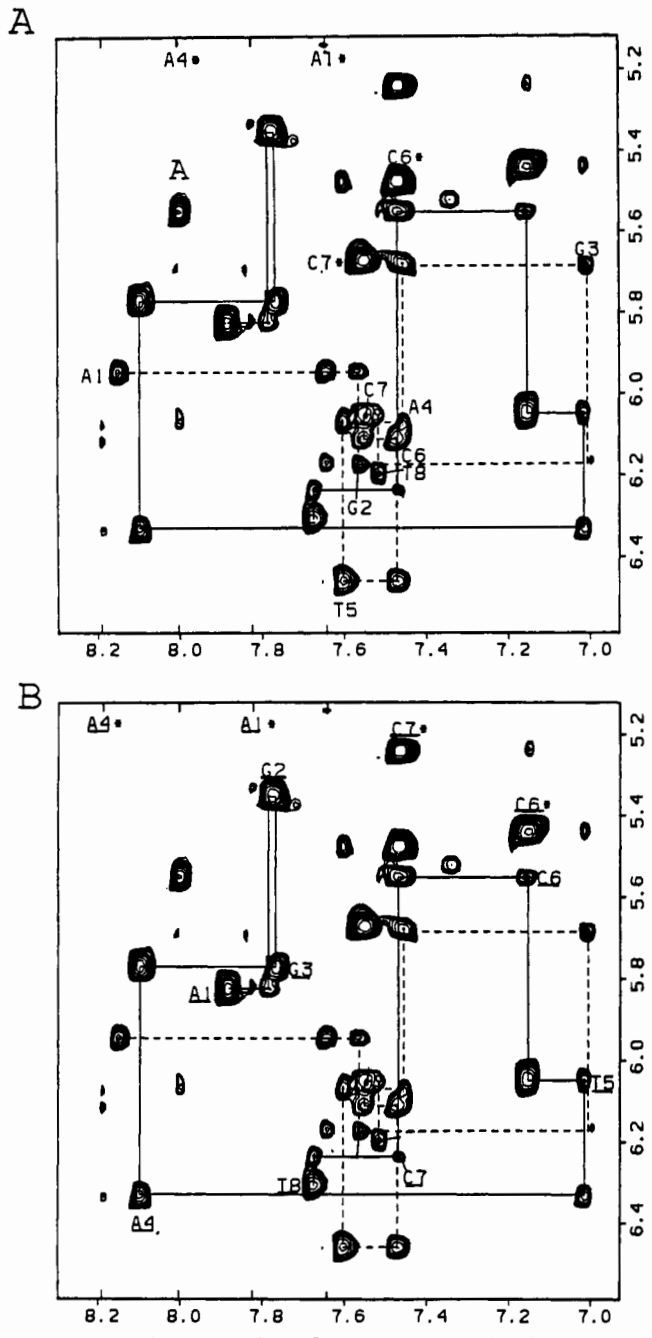

FIGURE 7: Duplicate expanded NOESY (250-ms mixing time) contour plots establishing distance connectivities between the base protons (7.0–8.2 ppm) and the sugar H1′ and cytidine H5 protons (5.2–6.6 ppm) for the Mg(II)-coordinated chromomycin–d(AG_2ATC_2T) complex in D_2O buffer, pH 7.4, at 25 °C. The chain is traced with dashed lines in the A1-G2-G3-A4-T5-C6-C7-T8 strand in (A), and the chain is traced with solid lines in the A1-G2-G3-A4-T5-C6-C7-T8 strand in (B). The cross peak labeled A corresponds to an NOE between A4(H2) and C6(H1′).

Figure 7A and for the d(A1-G2-G3-A4-T5-C6-C7-T8) strand in Figure 7B. It is readily apparent that there are dramatic chemical shift differences for the base and sugar H1′ protons for several sequence-symmetry-related positions in the two strands of the asymmetric chromomycin–d(AG_2ATC_2T) complex.

The complete nucleic acid nonexchangeable proton chemical shifts in the Mg(II)-coordinated chromomycin–d(AG_2ATC_2T) complex at 25 °C are listed in Table V and can be compared with the corresponding nonexchangeable proton chemical shifts in the self-complementary d(AG_2ATC_2T) duplex, which are listed in Table SVI (supplementary material). The most

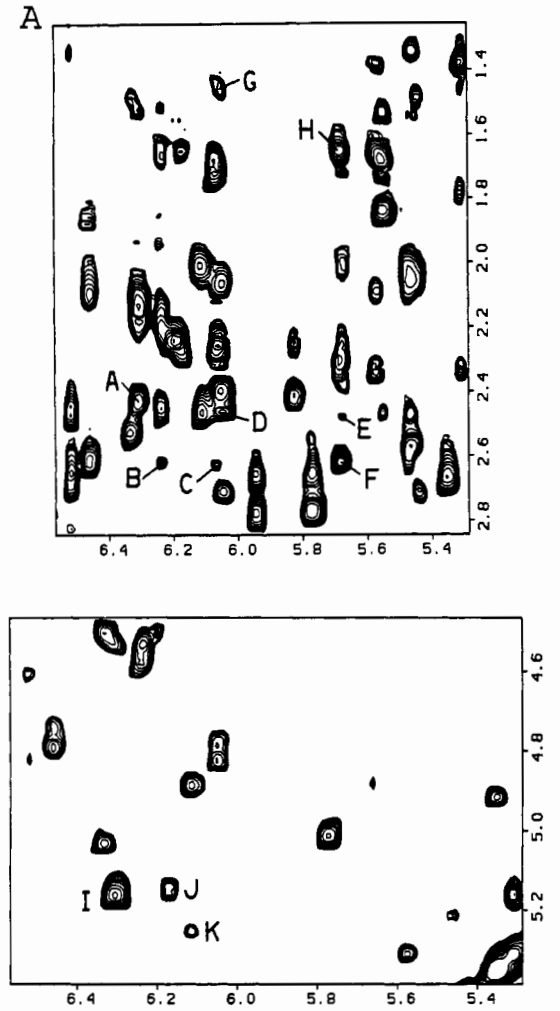

FIGURE 8: The 250-ms NOESY spectrum of the Mg(II)-coordinated chromomycin–d(AG_2ATC_2T) complex in D_2O buffer, 25 °C. (A) NOE cross peaks between the 5.2–6.6 ppm and 1.2–2.9 ppm regions. (B) NOE cross peaks between the 5.2–6.6 ppm and 4.4–5.4 ppm regions. The cross peaks A–K are assigned as follows: A, E-(H2)-T8(H1′); B, CHR(C7-CH_3)-C7(H1′); C, CHR(C7-CH_3)-A4(H1′); D, CHR(C7-CH_3)-T5(H1′); E, CHR(C7-CH_3)-C6(H1′); F, CHR(C7-CH_3)-G3(H1′); G, E(C6-CH_3)-T5(H1′); H, E(C6-CH_3)-G3(H1′); I, E(H1)-T8(H1′); J, E(H4)-G2(H1′); and K, E(H1)-C6(H1′).

dramatic complexation shifts were found for the A4 and C6 H4′ protons. Their chemical shifts of 1.67 and 1.54 ppm are upfield of the ~4 ppm chemical shifts for unperturbed H4′ protons.

Chromomycin Nonexchangeable Proton Shifts: The binding of individual chromomycin subunits introduces distinct chemical shifts in the asymmetric chromomycin–d(AG_2ATC_2T) complex. The NOESY (Figure S9B) and DQF-COSY contour plots for the complex can be analyzed to yield the proton chemical shifts of the individual chromomycins; these are listed in Table V. There are no pronounced chemical shifts differences between the chromomycin subunits labeled in normal and underlined print in the chromomycin dimer–d(AG_2ATC_2T) complex (Table V).

Intermolecular NOEs Involving Nonexchangeable Protons. Several intermolecular NOEs have been identified in the 250-ms mixing time NOESY spectrum of the chromomycin dimer–d(AG_2ATC_2T) complex at 25 °C. Expanded contour plots that establish distance connectivities between the 5.2–6.6 ppm region and the 1.2–2.9 ppm and 4.5–5.4 ppm regions are plotted in Figure 8, panels A and B, respectively. The relevant NOE cross peaks are labeled in the plot, and the assignments

Table VI: Major Intermolecular NOEs in Chromomycin–d(AG_2ATC_2T) Complex

chromomycin residue		d(AG_2ATC_2T) residue	H2	H1′	H4′	H5′,5″
		Strand I				
A-sugar[a]	H1	A4				w
aglycon[b]	H5	A4			w	
	CH_3-7	G3		s		
	CH_3-7	C7		w		
	OH8	A4	m			
E-sugar[c]	H1	C6		w		
	CH_3-6	T5		m		
		Strand II				
A-sugar	H1	C6			w	m
aglycon	H5	C6			w	
	CH_3-7	T5		s		
	CH_3-7	A4	w			
	OH8	A4	w			
	OH8	T5		w		
	OH8	C6		m		
E-sugar	H1	T8		s	w	
	H2a,e	T8		m		
	H4	G2		w		
	CH_3-6	G3		w		

[a] One chromomycin A-sugar interacts with the backbone of d(AG_2ATC_2T) at the G3-A4 step. [b] One aglycon binds to the G2·C7 and G3·C6 pairs with its hydrophilic edge facing the minor groove and its hydrophobic edge tilted toward the backbone. [c] One E-sugar resides in the minor groove at the T5·A4 and C6·G3 pairs. [d] The second chromomycin A-sugar interacts with the backbone of d(AG_2ATC_2T) at the T5-C6 step. [e] The second aglycon binds to the A4·T5 and T5·A4 pairs with its hydrophilic edge facing the minor groove and its hydrophobic edge tilted toward the backbone. [f] The second chromomycin E-sugar resides in the minor groove at the A1·T8 and G2·C7 pairs.

are listed in the caption to Figure 8A. The intermolecular NOEs are defined as weak, medium, and strong and are summarized in Table VI.

The alignments of the chromomycin aglycon rings in the complex are defined by the observed NOEs between the C7-CH_3 of CHR on one subunit and the H1′ of G3 (peak F, Figure 8A) on one strand and between the C7CH_3 of CHR on the other subunit and the H1′ of T5 (peak D, Figure 8A) on the partner strand. The alignment of one of the C-D-E trisaccharide segments can be defined by the observed NOEs between H1 and geminal H2 proton of the E-ring and the H1′ proton of T8 (peak I, Figure 8B, and peak A, Figure 8A, respectively) in the complex.

Phosphorus Spectra. The same pattern of both downfield and upfield complexation shifts is detected for the chromomycin complex with the d(AG_2ATC_2T) duplex (Figure S1B) as was observed for the complex with the d($A_2G_2C_2T_2$) duplex (Figure S1A).

Symmetric Zn(II)-Coordinated Complex

NMR Spectra. The chromomycin–d($A_2G_2C_2T_2$) complex (2 drug molecules per duplex) in the presence of 1 equiv of $ZnCl_2$ yields well-resolved exchangeable proton (Figure 9B) and phosphorus (Figure S10B, supplementary material) spectra in aqueous solution. These spectra of the Zn(II) complex are very similar to those of the Mg(II) complex. We note that the C8-hydroxyl proton of the chromomycin aglycon ring resonates at 15.75 ppm in the Zn(II) complex (Figure 9B), compared to 16.15 ppm in the Mg(II) complex (Figure 9A), so that this resonance provides a convenient marker for monitoring Mg(II)–Zn(II) cation exchange in the chromomycin–d($A_2G_2C_2T_2$) complex.

Thermal Melting. The 15.75 ppm C8-hydroxyl proton

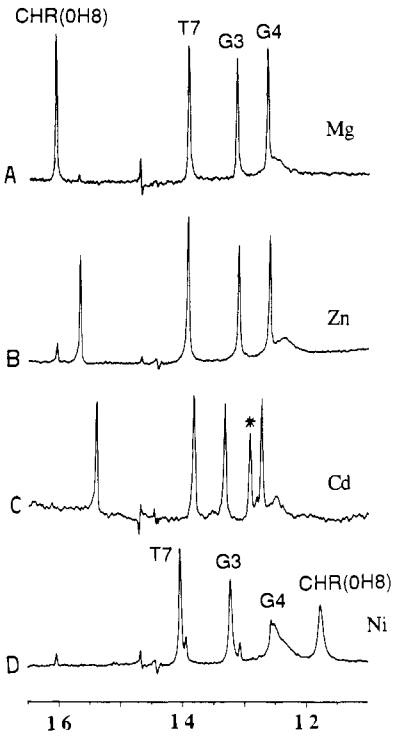

FIGURE 9: Proton NMR spectra (11.0–15.5 ppm) of the divalent cation coordinated chromomycin–d($A_2G_2C_2T_2$) complex (1 cation and 2 drug molecules per duplex) in 0.1 M NaCl and 10 mM phosphate in H_2O solution. (A) Mg(II) complex, pH 6.7, 25 °C. (B) Zn(II) complex, pH 6.7, 30 °C. (C) Cd(II) complex, pH 5.9, 25 °C. The asterisk indicates imino proton from free duplex. (D) Ni(II) complex, pH 7.0, 30 °C.

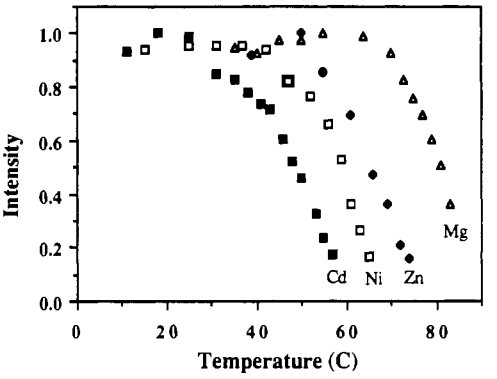

FIGURE 10: Thermal transition of the divalent cation coordinated chromomycin–d($A_2G_2C_2T_2$) complex in 0.1 M NaCl and 10 mM phosphate in H_2O solution. Melting curves are for the Mg(II), Zn(II), Cd(II), and Ni(II) complexes. The chromomycin aglycon C8-hydroxyl proton in the complex was used as a marker to monitor the transition. The transition for the Ni(II) complex was irreversible.

remains narrow (line width ~17 Hz) in the Zn(II)-coordinated chromomycin–d($A_2G_2C_2T_2$) complex on raising the temperature up to 80 °C. Under such conditions, the C8-hydroxyl resonance of free chromomycin (~18 ppm) is too broad to be detected. The intensity of the C8-hydroxyl proton hence serves as a suitable marker for monitoring the temperature-dependent dissociation of the complex in aqueous solution. The thermal melting curve of the Zn(II) complex yields a T_m = 65 °C, while that for the corresponding Mg(II) complex yields at T_m = 77 °C (Figure 10).

Divalent Cation Exchange in Complex. The 15.75 ppm C8-hydroxyl proton in the Zn(II) complex was used to monitor Mg(II) for Zn(II) exchange in the chromomycin–d($A_2G_2C_2T_2$) complex in H_2O buffer, pH 5.6, at 25 °C. The intensity of the 15.75 ppm resonance was recorded as a function of time

Table VII: Parameter Comparisons of Divalent Cation Coordinated Chromomycin–d($A_2G_2C_2T_2$) Complexes[a]

	Mg(II)	Ni(II)	Zn(II)	Cd(II)
chemical shift[b] (ppm)	16.15	12.94	15.75	15.40
T_m[c] (°C)	77	59	65	48
$T1$(real-life time)[d] (h)	>63	infinite	2.8	<0.25
$T1$[Zn(II) → Mg(II)][e] (h)	61			
$T1$[Mg(II) → X(II)][f] (h)		infinite	2.4	<0.25

[a] Each of the complexes is represented in the table by the corresponding metal ion used to generate the complex. [b] Chemical shift of the C8-hydroxyl proton resonance of chromomycin at 25 °C. [c] T_m is the melting temperature (±2 °C) where intensity of the CHR(OH8) resonance decreases to half the initial intensity. The pH was 6.4 ± 0.1 for all samples, except for the Cd(II) complex, which is only stable at pH 5.9 or lower. [d] Time constants of the real-life time of CHR(OH8) in the complex measured in D_2O buffer solution at room temperature and pH 6.4–7.0, except for the Cd(II) complex, which was measured at pH 5.6. [e] Time constants of the exchange between free Zn(II) (10 equiv) and bound Mg(II) in the complex. [f] Time constants of the metal ion exchange between free Mg(II) (10 equiv) and bound metal ion in a particular complex as monitored by intensity variations of the CHR(OH8) resonance in the complex. pH conditions: Ni(II), pH 7.0; Zn(II), pH 5.6; and Cd(II), pH 5.9.

in a solution of the Zn(II) complex in the presence of a 10-fold excess of Mg(II) ions. The replacement by Mg(II) of Zn(II) in the complex can be monitored by the exponential decay of the intensity of the 15.75 ppm resonance with a time constant of 2.4 h (Figure S11A, supplementary material, and Table VII).

A parallel study has investigated replacement by Zn(II) of Mg(II) in the chromomycin–d($A_2G_2C_2T_2$) complex at 25 °C. The exchange was studied on the Mg(II) complex in the presence of a 10-fold excess of Zn(II) by monitoring the buildup of the 15.75 ppm C8-hydroxyl resonance characteristic of the Zn(II) complex. The Zn(II) for Mg(II) exchange in the complex exhibits a time constant of 61 h, which is a factor of 23 longer than the corresponding Mg(II) for Zn(II) exchange in the complex (Table VII).

Real-Time Exchange. The amino protons of G3 and G4, along with the aglycon C8-hydroxyl proton, provide suitable markers for monitoring real-time exchange when a sample of Zn(II)-coordinate chromomycin–d($A_2G_2C_2T_2$) complex (all exchangeable protons protonated) is freshly dissolved in D_2O solution. Of these three markers, the proton to deuterium exchange occurs faster for the G3 amino protons relative to the G4 amino protons and aglycon C8 hydroxyl proton in the complex. The real-time proton to deuterium exchange for the 15.75 ppm aglycon C8-hydroxyl proton of the Zn(II) complex exhibits a time constant of 2.8 h at pH 6.7 and 25 °C (Figure S11B, supplementary material, and Table VII). By contrast, the proton to deuterium exchange of the C8-hydroxyl proton in the Mg complex exhibits a time constant of >63 h at pH 6.7 and 25 °C (Table VII).

Symmetric Cd(II)-Coordinated Complex

Conditions. Attempts to generate the chromomycin–d($A_2G_2C_2T_2$) complex (2 drug molecules per duplex) in the presence of up to a 5-fold excess of $CdCl_2$ were unsuccessful at neutral or alkaline pH. However, the complex could be generated on lowering the pH. This pH-dependent equilibrium between the Cd(II)-coordinated complex and its dissociated components was reversible, with 80% complex formation estimated at pH 5.9.

NMR Spectra. The exchangeable proton (Figure 9C) and phosphorus (Figure S10C, supplementary material) spectra of the Cd(II)-coordinated chromomycin–d($A_2G_2C_2T_2$) complex, pH 5.9, at 25 °C exhibit well resolved resonances. The C8-hydroxyl proton in the Cd(II) complex resonates at 15.40 ppm (Figure 9C) and can be readily distinguished from the corresponding 16.15 ppm resonance in the Mg(II) complex (Figure 9A).

Equilibrium and Kinetic Parameters. The thermal melting transition of the Cd(II) complex has been monitored by using the 15.40 ppm C8-hydroxyl proton as a marker and exhibits a T_m = 48 °C at pH 5.9 (Figure 10).

The kinetics of divalent metal ion exchange, as well as real-time solvent exchange measurements, have been undertaken on the Cd(II)-coordinated chromomycin–d($A_2G_2C_2T_2$) complex at pH 5.9. Metal ion exchange of Cd(II) in the Cd(II) complex by a 10-fold excess of Mg(II) exhibits a time constant of <0.25 h at 25 °C (Table VII). Similarly, a time constant of <0.25 h is estimated for real-time proton to deuterium exchange of the C8-hydroxyl proton for the Cd(II) complex when dissolved in D_2O solution, pH 5.6, at 25 °C (Table VII).

Symmetric Ni(II)-Coordinated Complex

NMR Spectra. We have been able to readily generate the chromomycin–d($A_2G_2C_2T_2$) complex (2 drug molecules per duplex) in the presence of 1 equiv of $NiCl_2$ in aqueous solution. In contrast to Mg(II) and Zn(II), which are diamagnetic divalent cations, Ni(II) is paramagnetic and has the potential for shifting and broadening proton resonances in its immediate vicinity. The exchangeable proton (Figure 9D) and phosphorus (Figure S10D, supplementary material) spectra of the Ni(II) complex exhibit both shifted and broadened resonances compared to their counterpart spectra for the Mg(II) complex.

The C8-hydroxyl chromomycin proton resonates at 12.94 ppm in the Ni(II) complex (Figure 9D); this represents an ~3 ppm upfield shift along with increased broadening when compared to its position and width in the Mg(II) complex (Figure 9A). The imino proton of G4 is significantly broadened, while the hydrogen-bonded amino proton of G4 cannot be detected in the Ni(II) complex. Similarly, distinct nonexchangeable proton and phosphorus chemical shift and line width changes are detected on comparison of spectra for the paramagnetic Ni(II) complex with the corresponding diamagnetic Mg(II) complex.

Spin–Lattice Relaxation Times. The presence of a paramagnetic divalent cation in the Ni(II) complex greatly enhances the spin–lattice relaxation rate of nonexchangeable protons depending on the metal cation to proton distances. The spin–lattice relaxation time ($T1$) values of base and sugar protons are in the 1.3-s range (except the H2 of adenosine, which exhibits a longer $T1$) for one-turn-of-helix DNA oligomer duplexes. By contrast, for the Ni(II) complex, most protons have $T1$ values shorter than 150 ms, while others relax so fast ($T1$ < 45 ms) that no cross peaks originating in these resonances can be detected in two-dimensional NMR data sets. We have measured nonselective $T1$ values by inversion recovery experiments on a number of observable and resolved protons in the Ni(II) complex at 25 °C; these are listed in Table VIII.

NOESY Spectra. The NOESY data set on the Ni(II)-coordinated chromomycin–d($A_2G_2C_2T_2$) complex in D_2O buffer, pH 7.0, at 25 °C was recorded with a mixing time of 170 ms. This mixing time value was chosen as a compromise between the long mixing time required for NOE buildup and the short mixing times required to limit relaxation of the magnetization due to the paramagnetic cation. An expanded 170-ms mixing time NOESY contour plot establishing distance connectivities between the 4.8–8.5 ppm and 0.8–3.6 ppm regions of the paramagnetic Ni(II) complex at 25 °C is plotted

Table VIII: $T1$ Values for Ni(II)-Coordinated Chromomycin–$d(A_2G_2C_2T_2)$ Complex[a]

resonances	$T1$ (ms)	distance[b] (Å)
CHR(OH8), G4(1′), C5(1′)	<44	<8.5
T7(H6)	44	10.1
G4(H8)	73	10.3
T7(H1′)	101	12.1
A2(H8), G3(H8)	145	>13.0
G3(H1′)	159	12.2

[a] Nonselective $T1$ of selected resolved resonances determined by inversion recovery experiment; buffer contains 0.1 M NaCl, 10 mM phosphate and 1 equiv of added $NiCl_2$ in D_2O, pH 7.0, at 20 °C. [b] Distance derived from refined model of the complex (Gao, Mirau, and Patel, manuscript in preparation).

in Figure 11B. As a control, the corresponding expanded 250-ms NOESY contour plot of the same region in the diamagnetic Mg(II) complex at 25 °C is plotted in Figure 11A. The relevant cross peaks are labeled in either panel A or panel B or are explained in the Figure 11 caption. We detect the majority of the NOE cross peaks corresponding to proton resonances of A1, A2, G3, T7, and T8 nucleic acid residues and the A-, B-, and E-sugar rings of the antitumor agent in the Ni(II)-coordinated chromomycin–$d(A_2G_2C_2T_2)$ complex (Figure 11B). By contrast, no NOE cross peaks are detected associated with protons on G4, C5, and C6 nucleic acid residues and the aglycon and C- and D-sugar rings on the antitumor agent in the Ni(II) complex (Figure 11B). These observations establish which residues on the chromomycin and the DNA octanucleotide duplex are close to the paramagnetic divalent ion in the Ni(II) complex in solution. The observable and assignable proton chemical shifts in the Ni(II) complex are listed in Table IX.

Equilibrium and Kinetic Parameters. The 11.88 ppm C8-hydroxyl proton was used to monitor the melting of the Ni(II)-coordinated chromomycin–$d(A_2G_2C_2T_2)$ complex. A T_m of 59 °C was observed for the Ni(II) complex (Figure 10), but the reliability of this value is in question due to the irreversibility of the melting transition. This may reflect the oxidation of the Ni(II) cation at elevated temperatures.

The 11.88 ppm C8-hydroxyl proton was used to monitor the exchange of Ni(II) by a 10-fold excess of Mg(II) ions in the Ni(II) complex. This exchange is too slow to measure since no change was detected in the intensity of this resonance after several days at 25 °C (Table VII). Similarly, the real-time exchange of the 11.88 ppm C8-hydroxyl proton of the Ni(II) complex could not be detected after 5 days in D_2O, pH 6.7, at 25 °C (Table VII).

Other Metal Cation Complexes

Diamagnetic Divalent Cations. We were unable to generate the chromomycin–$d(A_2G_2C_2T_2)$ complex in the presence of Ca(II) ions.

Paramagnetic Divalent Cations. We detected dramatic line broadening of the proton resonances of the complex on addition of Mn(II) ions at low stoichiometric ratios, precluding characterization of the role of Mn(II) coordination in the complex.

Dramatic complexation shifts with some broadening were detected for nonexchangeable proton and phosphorus spectra of the chromomycin–$d(A_2G_2C_2T_2)$ complex (2 drug molecules per duplex) in the presence of paramagnetic $Co(II)Cl_2$. Thus, nonexchangeable protons are dispersed over 80 ppm (Figure S12B, supplementary material; broad resonances at 47 and −39 ppm are not shown) and the phosphorus resonances are dispersed over 13 ppm. By contrast, proton resonance perturbations were not observed when 0.35 equiv of $Co(II)Cl_2$ was added to the $d(A_2G_2C_2T_2)$ duplex.

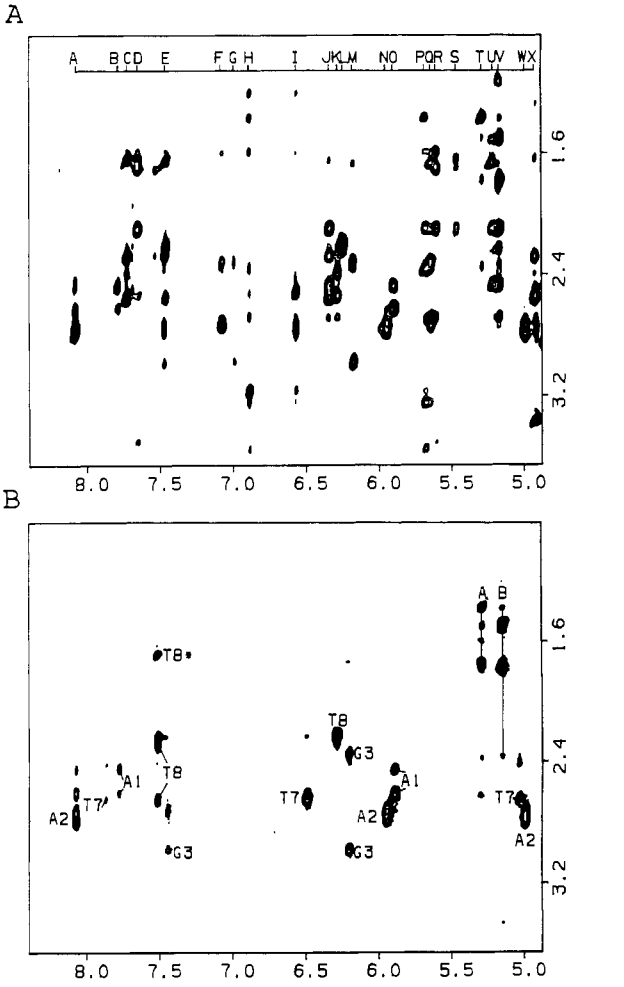

FIGURE 11: Expanded NOESY plots establishing distance connectivities between the 5.0–8.5 ppm and 1.0–3.6 ppm regions in the divalent cation coordinated chromomycin–$d(A_2G_2C_2T_2)$ complex in D_2O buffer. (A) 250-ms NOESY plot of Mg(II)-coordinated complex at 25 °C. (B) 170-ms NOESY plot of Ni(II)-coordinated complex at 25 °C. The letters A–X in (A) correspond to assigned protons as follows: A, A2(H8); B, A1(H8); C, T7(H6); D, C6(H6); E, G3(H8), T8(H6); F, C5(H6); G, G4(H8); H, CHR(H5); I, CHR(H10); J, T7(H1′); K, C6(H1′); L, T8(H1′); M, G3(H1′); N, A2(H1′); O, A1(H1′); P, A(H1); Q, G4(H1′); R, C5(H1′); S, C6(H5); T, A(H4); U, E(H4); V, B(H1), E(H1); W, A2(H3′); and X, T7(H3′). The letters in (B) correspond either to nucleic acid cross peaks of residues A1, A2, G3, T7, and T8 or to chromomycin cross peaks of saccharide residues A and B.

DISCUSSION

Stoichiometry and Chromomycin Dimer Formation. The gradual addition of chromomycin to the self-complementary $d(A_2G_2C_2T_2)$ and $d(AG_2ATC_2T)$ duplexes in solution containing 1 equiv of Mg(II) establishes that the stoichiometry of complex formation is 2 equiv of antitumor agent bound per duplex, with no evidence for complexes containing 1 equiv of antitumor agent bound per duplex.

We reasoned that a comparative NMR study of the symmetry properties of chromomycin (2 equiv) complexes with the self-complementary $d(A_2G_2C_2T_2)$ and $d(AG_2ATC_2T)$ duplexes should distinguish between the antitumor agent binding as a dimer or as a pair of independent monomers. Previous studies have established that each chromomycin subunit preferentially binds to the (G-G)·(C-C) step (Gao & Patel, 1989), so that both subunits could bind either as a dimer or as two independent monomers to the central (G-G-C-C)·(G-G-C-C) segment of the $d(A_2G_2C_2T_2)$ duplex with retention of 2-fold symmetry. This is exactly what is observed,

Table IX: Proton Chemical Shifts (ppm) in the Ni(II)-Coordinated Chromomycin–d($A_2G_2C_2T_2$) Complex

d($A_2G_2C_2T_2$) Protons												
nucleotide	NH	NH_2		H8	H2	H6	H5	H1′	H2′	H2″	H3′	H4′	H5′,5″
A1				7.77				5.90	2.44	2.62	4.81	4.16	3.68
A2				8.07	7.72			5.96	2.80	2.71	4.98	4.41	4.13
G3	13.24	9.65	6.30	7.44				6.21	2.98	2.35	4.63	4.30	
G4	12.52	***	***	6.84?				*	*	*	4.10?		
C5		*	*			**	*	***	**	***	**	**	
C6		*	*			**	*	**	*	**	*	**	
T7	14.08					7.85	*	6.50	2.39	2.65	5.03		
T8						7.51	1.71	6.29	2.25	2.25	4.59	4.00	4.10

Chromomycin Saccharide Protons									
sugar	H1	H2(a)	H2(e)	H3	H4	H5	H6	Ac	OCH_3
A	5.64	2.18		4.33	5.28	4.09	1.38	2.36	
B	5.14	1.77	1.51	4.07	3.46	3.84	1.21		3.52
C	***	**	**	**	*	**	**		
D	**	*	*	*		3.14	1.21		
E	*	2.61	2.24	1.61	5.30	4.41	1.75	2.25	

Chromomycin Aglycon Protons												
aglycon	H2	H3	H4	H5	H7	H10	H1′	H1′(OMe)	H3′	H4′	H5′	OH8
CHR	**	**	** **	6.94?	2.62?	**	**	*	*	*		11.94

[a] Buffer solution contains 0.1 M NaCl, 10 mM phosphate, and 1 equiv of $NiCl_2$. The nonexchangeable proton data were obtained in D_2O, pH 7.0, at 25 °C; the exchangeable proton data were obtained in H_2O, pH 7.0, at 20 °C. In the table, * covers distance range of $d < 4$ Å, ** covers 4 Å < $d < 7$ Å, and *** covers 7 Å < $d < 10$ Å, defined from the refined model of the Mg(II)-coordinated complex (Gao, Mirau, and Patel, manuscript in preparation). ? represents proposed cross peak assignments that do not exhibit NOE connectivity due to paramagnetic broadening of Ni(II) in the complex.

as shown in the exchangeable proton (Figure 1A) and phosphorus (Figure S1A) spectra of the chromomycin–d($A_2G_2C_2T_2$) complex [1 Mg(II) and 2 drugs per duplex] in aqueous solution.

By contrast, the (G-G)·(C-C) steps are separated by two A·T pairs in the self-complementary d(AG_2ATC_2T) duplex, so that different results are expected depending on whether the 2 equiv of chromomycin bind as a dimer or as a pair of independent monomers. Experimentally, the exchangeable proton (Figure 1B) and phosphorus (Figure S1B) spectra and intermolecular contacts (Table VI) establish that the 2-fold symmetry of the self-complementary d(AG_2ATC_2T) duplex is lifted on addition of 2 equiv of chromomycin and that only one (G-G)·(C-C) site in the duplex interacts with the bound chromomycin. This is consistent with the antitumor agent binding as a dimer rather than as a pair of independent monomers.

Guanosine Amino Protons as Markers for Minor-Groove Recognition. We have observed the major-groove cytidine amino protons and the minor-groove guanosine amino protons for the G4·C5 and G3·C6 base pairs in the Mg(II)-coordinated chromomycin–d($A_2G_2C_2T_2$) complex (Figure 2A). Furthermore, separate resonances are detected for the hydrogen-bonded and exposed amino protons of guanosine and of cytidine in each case. The guanosine amino protons can be distinguished from the cytidine amino protons since the former exhibit NOEs to nearby sugar H1′ protons in the minor groove, while the latter exhibit NOEs to cytidine H5 protons in the major groove. The observation of hydrogen-bonded and exposed amino protons of G3 and G4 was unexpected and establishes that the intermediate rotation rate about the C–NH_2 bond of G residues in the free duplex (Patel, 1976) switches to slow rotation about this bond in the chromomycin complex.

The 16.15 ppm chromomycin C8-hydroxyl proton exhibits NOEs to the exposed and hydrogen-bonded amino protons of G4, with a stronger magnitude to the former (peak K, Figure 2A) compared to the latter (peak J, Figure 2A) amino protons in the chromomycin–d($A_2G_2C_2T_2$) complex. Furthermore, the C7-CH_3 protons exhibit NOEs to the 13.24 ppm imino and 9.53 ppm hydrogen-bonded amino protons of G3 in the complex. These NOEs establish that the chromomycin dimer is centered about the (G3-G4-C5-C6)·(G3-G4-C5-C6) segment, resulting in a symmetric positioning of the antitumor agent in the minor groove of the d($A_2G_2C_2T_2$) octanucleotide, as shown schematically in **2**.

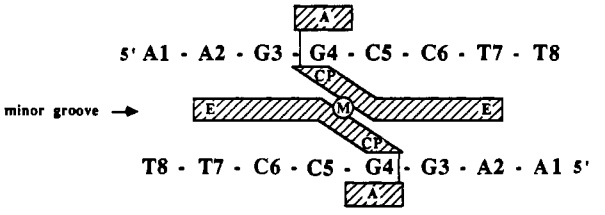

2

We detect separate hydrogen-bonded and exposed guanosine amino protons for the G2·C7 and G3·C6 base pairs but not for the G2·C7 and G3·C6 base pairs in the Mg(II)-coordinated chromomycin–d(AG_2ATC_2T) complex (Figure 6). These results establish intermolecular contacts between the aglycon subunits in the chromomycin dimer and the minor groove for the G2-G3 step but not for the G2-G3 step on formation of the asymmetric chromomycin–d(AG_2ATC_2T) complex.

Intermolecular NOEs are observed between the 16.34 ppm C8-hydroxyl proton of one aglycon and the hydrogen-bonded and exposed amino protons of G3 (peaks A and C, Figure 6) and between the 14.95 ppm C8-hydroxyl proton of the other aglycon and the H2 proton of A4 (peak E, Figure 6) in the complex. These results establish that the hydrophilic edge of one aglycon subunit (CHR) contacts the minor groove positioned about the G3·C6 pair while the other aglycon subunit (CHR) of the chromomycin dimer contacts the minor groove positioned about the A4·T5 pair in the chromomycin–d(AG_2ATC_2T) complex. These NOEs establish that the chromomycin dimer is centered about the (G2-G3-A4-T5)·(A4-T5-C6-C7) segment, resulting in an asymmetric positioning of the antitumor agent dimer in the minor groove of the DNA octanucleotide duplex, as shown schematically in **3**.

Sequence Selectivity. A range of intermolecular NOEs are observed between the aglycon C8-hydroxyl and C7-methyl

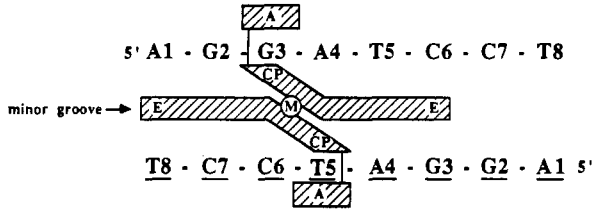

3

protons of the chromomycin and the minor-groove sugar H1′ and H4′ protons of G4, C5, and C6 residues on the d-($A_2G_2C_2T_2$) duplex in the complex (Table IV). A different set of intermolecular NOEs are detected between the protons on the E-saccharide ring of chromomycin and the minor-groove sugar H1′ and H4′ protons of G3, G4, and T7 residues on the d($A_2G_2C_2T_2$) duplex in the complex (Table IV). These results establish that the chromomycin dimer interacts in the minor groove with both strands of the d($A_2G_2C_2T_2$) duplex such that its binding site covers the (G3-G4-C5-C6-T7)·(G3-G4-C5-C6-T7) segment (**2**). This conclusion is reinforced by the observation of significant base and sugar proton complexation shifts for the G3, G4, C5, C6, and T7 positions on formation of the chromomycin–d($A_2G_2C_2T_2$) complex (Figure S13A, supplementary material).

The observed intermolecular NOEs (Table VI) permit alignment of the chromomycin dimer asymmetrically at the (G2-G3-A4-T5-C6)·(A4-T5-C6-C7-T8) segment of the d-(AG_2ATC_2T) duplex on complex formation. One chromomycin aglycon ring interacts with the G2-G3 step and its C-D-E trisaccharide segment extends over the A4-T5-C6 segment, while the other chromomycin aglycon ring interacts with the A4-T5 step and its C-D-E trisaccharide segment extends over the C6-C7-T8 segment. The asymmetric alignment of the chromomycin dimer on the (AG_2ATC_2T) duplex (**3**) is supported by the observation of selective base and sugar proton complexation shifts at the G2, G3, A4, and T5 positions on one of the strands (Figure S13B, top) and at the T5, C6, and C7 positions on the other strand (Figure S13B, bottom) on formation of the chromomycin–d(AG_2ATC_2T) complex.

Our studies detect strong binding of each aglycon ring in the chromomycin dimer at its respective (G-G)·(C-C) half-site on the (G-G-C-C)·(G-G-C-C) segment in the chromomycin–d($A_2G_2C_2T_2$) complex. By contrast, we observe that binding of the aglycon of one chromomycin subunit at the preferred (G-G)·(C-C) half-site assists in the binding of the aglycon of the other chromomycin subunit at an otherwise unfavorable (A-T)·(A-T) half-site in the (G-G-A-T)·(A-T-C-C) segment in the chromomycin–d(AG_2ATC_2T) complex.

Divalent Cation Binding Site(s). Divalent metal ion titration studies establish that chromomycin–d($A_2G_2C_2T_2$) complex formation has an absolute requirement for a single coordinated Mg(II) ion. This divalent cation is tightly coordinated and cannot be removed by added ethylenediaminetetraacetic acid (EDTA) chelating agent up to 10 equiv.

The divalent cation coordination site can be probed by a systematic comparison of the C8-hydroxyl proton chemical shift in complexes containing different cations. The observed variation in C8-hydroxyl proton shifts for the Mg(II) (16.15 ppm), Zn(II) (15.75 ppm), Cd(II) (15.40 ppm), and Ni(II) (12.94 ppm) complexes was not observed for other protons in the complex and provides strong evidence for the divalent cation coordination at the O9 and O1 positions.

The coordination site of the tightly bound divalent cation can also be probed by comparing two-dimensional data sets of the chromomycin–d($A_2G_2C_2T_2$) complex with diamagnetic Mg(II) as the counterion on the one hand (Figure 11A) and paramagnetic Ni(II) as the counterion on the other (Figure 11B). We do not detect NOE cross peaks involving protons on the aglycon and the C and D saccharide rings in the Ni(II) complex (Figure 11B), requiring the paramagnetic ion to be within 13 Å of these groups of the chromomycin dimer in the complex. These results are consistent with our earlier model (Gao & Patel, 1989), which proposed that the divalent ion coordination involves the C1 carbonyl and ionized C9 enolate of the aglycon ring and that the approximate orthogonal arrangement of the two aglycons in the chromomycin dimer provides four coordination sites for the divalent metal ion in the complex.

The exchangeable proton spectra of the chromomycin–d-($A_2G_2C_2T_2$) complex in the presence of Zn(II), Cd(II), and Ni(II) exhibit a weak signal corresponding to the 16.15 ppm aglycon C8-hydroxyl proton characteristic of the presence of a small amount of Mg(II) complex (Figure 9). We attribute this to the presence of a trace amount of Mg(II) in the buffers used to prepare the solutions. We propose an alternate explanation for an earlier claim that chromomycin binds to DNA in a nonionized form at acidic pH (Weinberger et al., 1988). This optical study was most likely conducted without completely removing Mg(II), and such effects become significant at the low concentrations used in the optical measurements.

The observed dependence of the chemical shifts and line widths of the major-groove H8 protons of G3 and G4 on lowering the pH of the chromomycin–d($A_2G_2C_2T_2$) complex in the presence of 1 equiv of Mg(II) (Figure 5, panels A and B) and further increases in line width with added Mg(II) and Mn(II) at acidic pH (Figure 5, panels C and D, respectively) establishes the selective protonation at the N7 positions of G3 and G4 at low pH and the presence of secondary divalent metal ion binding sites. We propose that these secondary sites involve divalent cation coordination to the major-groove N7 positions of G3-G4 steps in the complex. These divalent cation binding sites, which were not detected in the d($A_2G_2C_2T_2$) duplex, are weak in the complex since they can be eliminated by added EDTA chelating agent.

Thermal Stability. The melting transitions of the divalent cation coordinated chromomycin–d($A_2G_2C_2T_2$) complex are reversible in the case of the Mg(II), Zn(II), and Cd(II) complexes but not for the Ni(II) complexes. The T_m of the complex varies with divalent cation, with the thermodynamic stability decreasing in the order Mg(II) > Zn(II) > Cd(II) (Figure 10). Since the divalent cation is not directly involved in intermolecular interactions but rather in chromomycin dimer formation, these observations suggest an indirect effect of the metal cation on the stability of the complex. The variation in ionic radius and oxygen affinity of the various divalent cations could result in slightly different positioning of the coordinated aglycon chromophores, which in turn would modulate the intermolecular contacts in the complex. The divalent cation could coordinate by either tetrahedral or octahedral coordination, resulting in a variation in coordination geometry with divalent cation. Finally, electrostatic contributions about the cation binding site could vary with divalent metal ion and hence modulate the stability of the complex.

The relative exchange broadening of the imino protons with increasing temperature provides an estimate of the relative stability of the central G·C versus terminal A·T base pairs in the Mg(II)-coordinated chromomycin–d($A_2G_2C_2T_2$) complex. We note that the A2·T7 base pair broadens out at temperatures that are 50 °C below the dissociation temperature of the Mg(II) complex. It therefore appears that the Mg(II)-co-

ordinated chromomycin dimer stabilizes the fully protected central (G-G-C-C)·(G-G-C-C) segment at its binding site with decreased stabilization at the flanking A·T base pairs toward either end of the duplex.

Dissociation Kinetics of Chromomycin Dimer from Complex. We were interested in deducing whether divalent metal cation exchange between bound and free cations occurred following dissociation of the complex or through direct exchange via penetration into the intact complex. The cation exchange studies have been undertaken on the divalent cation coordinated chromomycin–d($A_2G_2C_2T_2$) complex in the presence of a 10-fold excess of another divalent cation, using the intensity of the aglycon C8-hydroxyl proton as a marker (Figure S11A). These studies establish that the Ni(II) complex is most kinetically stable to divalent metal cation exchange and that the order of decreasing kinetic stability is Ni(II) ≫ Mg(II) > Zn(II) > Cd(II) complex.

A parallel set of experiments have monitored the real-time exchange characteristics of the aglycon C8-hydroxyl proton in divalent cation coordinated chromomycin–d($A_2G_2C_2T_2$) complex (Figure S11B and Table VII) as a function of divalent cation. This hydroxyl proton undergoes rapid proton to deuterium exchange when free chromomycin is freshly dissolved in D_2O buffer solution. By contrast, the time constant for proton to deuterium exchange of this hydroxyl proton is longest for the Ni(II) complex and decreases in the order Ni(II) ≫ Mg(II) > Zn(II) > Cd(II) complex. The aglycon C8-hydroxyl proton is hydrogen bonded to the minor-groove edge of the G4·C5 pair in the divalent cation coordinated chromomycin–d($A_2G_2C_2T_2$) complex, so that hydrogen exchange is most likely preceded by the dissociation of the divalent cation coordinated chromomycin dimer from the complex.

Our observation of the same trend for divalent cation exchange kinetics and real-time hydrogen exchange kinetics as a function of divalent cation in the chromomycin–d($A_2G_2C_2T_2$) complex (Table VII) strongly suggests that divalent cation exchange between bound and free forms occurs following dissociation of the divalent cation coordinated chromomycin dimer from the complex.

Summary

Our previous NMR study demonstrated that the antitumor agent chromomycin binds as a symmetric divalent cation coordinated dimer to a wider and shallower minor groove centered about the (G-G-C-C)·(G-G-C-C) segment of a DNA oligomer duplex (Gao & Patel, 1989). These NMR studies identified the hydrogen bonding and van der Waals contacts between the aglycon chromophore and oligosaccharide side chains of the divalent cation coordinated chromomycin dimer and the symmetry-related adjacent (G-G)·(C-C) sites on the DNA. A molecular model of the complex was proposed that was consistent with available chemical shift, distance, and torsion angle constraints deduced from analysis of two-dimensional NMR data sets on the complex in aqueous solution. This model emphasized the important role of the divalent cation in aligning the individual aglycons to generate the chromomycin dimer and the contribution of the oligosaccharide–minor groove DNA interactions in stabilizing the complex (Gao & Patel, 1989). The present NMR study expands on these observations by focusing on questions relating to sequence selectivity and divalent cation specificity associated with chromomycin dimer–DNA complex formation.

We have undertaken comparative NMR studies on chromomycin dimer–DNA complexes in which the oligomer sequences contain symmetry-related (G-G)·(C-C) half-sites that are either adjacent to each other or separated by two A·T base pairs. These experiments demonstrate a hierarchy of chromomycin dimer binding sites on duplex DNA, with the current study on the chromomycin–d(A-G-G-A-T-C-C-T) complex establishing that the binding of one subunit of the chromomycin dimer at its preferred (G-G)·(C-C) half-site assists in the binding of the second subunit to the less preferred adjacent (A-T)·(A-T) half-site on the duplex.

The binding site and role of divalent cations in chromomycin dimer–DNA oligomer complexes has been elucidated by systematic structural and dynamics studies using diamagnetic and paramagnetic divalent cations. A comparative NMR study of the line widths and relaxation times for the diamagnetic Mg(II)- and paramagnetic Ni(II)-coordinated complexes identifies the divalent cation coordination site in the chomomycin dimer–d(A-A-G-G-C-C-T-T) complex. The individual monomers in the chromomycin dimer are aligned through coordination of the divalent cation to the C1 carbonyl and the C9 enolate anion on the hydrophilic edge of each aglycon ring. The type of divalent cation strongly influences both the thermal stability and the dissociation kinetics of the chromomycin dimer–DNA oligomer complexes. The thermal stability of the complexes decreases in the order Mg(II) > Zn(II) > Cd(II), while the dissociation lifetimes of the complex, as measured from divalent cation exchange, decrease in the order Ni(II) ≫ Mg(II) > Zn(II) > Cd(II).

Acknowledgments

We acknowledge discussions with Dr. R. Hosur on measurement of coupling constants and Dr. M. Gueron on divalent cation coordination and cation exchange properties in the complex.

Supplementary Material Available

Figures S1–S13 and Tables SI–SVI, described in detail in the text (22 pages). Ordering information is given on any current masthead page.

Registry No. d(AAGGCCTT), 130032-67-6; d(AGGATCCT), 84757-68-6; chromomycin A_3, 7059-24-7; Mg(II)–chromomycin–d(AAGGCCTT) complex, 130063-27-3; Mg(II)–chromomycin–d(AGGATCCT) complex, 130144-30-8; Zn(II)–chromomycin–d(AAGGCCTT) complex, 130063-29-5; Cd(II)–chromomycin–d(AAGGCCTT) complex, 130063-31-9; Ni(II)–chromomycin–d(AAGGCCTT) complex, 130063-33-1; Co(II)–chromomycin–d(AAGGCCTT) complex, 130063-35-3.

References

Banville, D. L., Keniry, M. A., Kam, M., & Shafer, R. H. (1990) *Biochemistry 29*, 6521–6534.

Behr, W., Honikel, K., & Hartmann, G. (1969) *Eur. J. Biochem. 9*, 82–92.

Cons, B. M., & Fox, K. R. (1989) *Nucleic Acids Res. 17*, 5447–5459.

Fox, K., & Howarth, N. R. (1985) *Nucleic Acids Res. 13*, 8695–8714.

Gao, X., & Jones, R. A. (1987) *J. Am. Chem. Soc. 109*, 46–54.

Gao, X., & Patel, D. J. (1989) *Biochemistry 28*, 751–762.

Gause, G. F. (1974) in *Antibiotics III, Mechanism of Action of Antimicrobial and Antitumor Agents* (Corcoran, J. W., & Hahn, F. E., Eds.) pp 197–202, Springer-Verlag, Heidelberg, FRG.

Haasnoot, C. A., Waterink, H. P., van der Marel, G. A., & van Boom, J. H. (1984) *J. Biomol. Struct. Dyn. 2*, 345–360.

Keniry, M. A., Brown, S. C., Berman, E., & Shafer, R. H. (1987) *Biochemistry 26*, 1058–1067.

Kennedy, B. J., Yarbo, J. W., Kickertz, V., & Sandberg-

Wollheim, M. (1968) *Cancer Res. 28*, 91-97.
Miyamoto, M., Morita, K., Kawatmu, Y., Noguchi, S., Marumato, R., Tanaka, K., Tatsuck, S., Nakanishi, K., Nakadaira, Y., & Bhacca, N. S. (1964) *Tetrahedron Lett.*, 2355-2377.
Patel, D. J. (1976) *Biopolymers 15*, 533-558.
Thiem, Y., & Meyer, B. (1979) *J. Chem. Soc., Perkin Trans. 2*, 1331-1336.
Van Dyke, M. W., & Dervan, P. B. (1983) *Biochemistry 22*, 2373-2377.
Ward, D. C., Reich, E., & Goldberg, I. H. (1965) *Science 149*, 1259-1263.
Weinberger, S., Shafer, R., & Berman, E. (1988) *Biopolymers 27*, 831-842.
Zagorski, M., & Norman, D. (1989) *J. Magn. Reson. 83*, 167-172.

Mechanism of Adenylate Kinase. Critical Evaluation of the X-ray Model and Assignment of the AMP Site†

Honggao Yan, Terri Dahnke, Binbing Zhou, Atsushi Nakazawa,‡ and Ming-Daw Tsai*
Department of Chemistry and Ohio State Biochemistry Program, The Ohio State University, Columbus, Ohio 43210
Received May 24, 1990; Revised Manuscript Received August 28, 1990

ABSTRACT: The substrate binding sites of adenylate kinase (AK) proposed by X-ray crystallographic studies [Pai, E. F., Sachsenheimer, W., Schirmer, R. H., & Schulz, G. E. (1977) *J. Mol. Biol. 114*, 37-45, and subsequent revisions] were evaluated by site-specific mutagenesis in conjunction with structural analysis by NMR. The residues examined in this report include two near an adenosine site (threonine-39 and arginine-44) and two in the phosphate binding region (arginine-128 and arginine-149). The results and conclusions are summarized as follows: (a) *Although Thr-39 is very close to an adenine site* [Egner, U., Tomasselli, A. G., & Schulz, G. E. (1987) *J. Mol. Biol. 195*, 649-658], *it is nonessential either structurally or functionally.* (b) The R44M mutant enzyme showed significant increases in the Michaelis and dissociation constants of adenosine 5′-monophosphate (AMP) (36- and 22-fold, respectively) while all other kinetic parameters were relatively unperturbed. The proton NMR property of this mutant was unchanged in the free enzyme and only slightly perturbed in the binary complexes with AMP and with MgATP (adenosine 5′-triphosphate), and in the ternary complex with $MgAP_5A$ [P^1,P^5-bis(5′-adenosyl) pentaphosphate]. These results indicate that *Arg-44 interacts specifically with AMP starting at the binary complex, and suggest that the MgATP site proposed by Pai et al. (1977) is likely to be the AMP site.* (c) The kinetic parameters of R149M were dramatically perturbed: k_{cat} decreased by a factor of 1540, K_m increased to 130-fold, and k_{cat}/K_m decreased by a factor of 2×10^5. The structure was also unperturbed in the free enzyme and slightly perturbed in the $MgAP_5A$ complex. These results led to the conclusion that Arg-149 stabilizes the ternary complex by 2.9 kcal/mol and the transition state by 7.3 kcal/mol. Thus, *Arg-149 is also a critically important residue in the catalysis by AK.* (d) The k_{cat}, K_m, and dissociation constant of R128A were all perturbed to a small extent (within factors of 10-20). The proton NMR was also perturbed to a small extent in the free enzyme and in binary and ternary complexes. Thus, the structural and/or functional roles of Arg-128 are minor. (e) One set of AP_5A resonances (the set assigned to site I previously) was assigned to the AMP site on the basis of two findings: (i) the adenine-I H_2 of $MgAP_5A$ and the adenine H_2 of AMP were both shifted downfield (by 0.8 and 0.4 ppm, respectively) upon binding to AK, while the shifts of other adenine protons of AMP, MgATP, and $MgAP_5A$ were all <0.15 ppm upon binding to AK; (ii) the adenine-I H_8 of R44M+$MgAP_5A$ was perturbed by 0.09 ppm relative to that of WT+$MgAP_5A$ while all other adenine protons were unperturbed. (f) The results are used to critically evaluate existing binding site models, including the most recent addition by Kim et al. [Kim, H. J., Nishikawa, S., Tokutomi, Y., Takenaka, H., Hamada, M., Kuby, S. A., & Uesugi, S. (1990) *Biochemistry 29*, 1107-1111].

It is hard to believe that, for an enzyme as small, common, and extensively studied as adenylate kinase (AK),[1,2] little has been firmly established about how it catalyzes the reaction or even just where and how it binds to substrates. Ironically, AK is often considered as a typical kinase or ATP binding protein,

† This work was supported by a grant from the National Science Foundation (DMB-8904727). This study made use of a Bruker AM-500 NMR spectrometer at The Ohio State University, funded by NIH Grant RR01458, and the National Magnetic Resonance Facility at Madison, supported by NIH Grants RR02301 and RR02781 and NSF Grant DMB-8415048. This is paper 8 in the series "Mechanism of Adenylate Kinase". For paper 7, see Yan et al. (1990).
‡ Present address: Department of Biochemistry, Yamaguchi University School of Medicine, Ube, Japan.

[1] Abbreviations: ADP, adenosine 5′-diphosphate; AK, adenylate kinase; AMP, adenosine 5′-monophosphate; AP_5A, P^1,P^5-bis(5′-adenosyl) pentaphosphate; ATP, adenosine 5′-triphosphate; 1D, one dimensional; 2D, two dimensional; DTT, dithiothreitol; EDTA, ethylenediaminetetraacetate; FID, free induction decay; HEPES, *N*-(2-hydroxyethyl)-piperazine-*N*′-2-ethanesulfonic acid; NMR, nuclear magnetic resonance; NOE, nuclear Overhauser effect; NOESY, nuclear Overhauser enhanced spectroscopy; PAGE, polyacrylamide gel electrophoresis. SDS, sodium dodecyl sulfate; Tris, 2-amino-2-(hydroxymethyl)-1,3-propanediol; WT, wild type.

0006-2960/90/0429-10956$02.50/0